Thermorelaxing multicomponent flows investigated with a Baer-Nunziato-type model

Chao Zhang [1,*] and Lifeng Wang [1,2,†]
[1] *Institute of Applied Physics and Computational Mathematics, Beijing 100094, China*
[2] *Center for Applied Physics and Technology, HEDPS, Peking University, Beijing 100871, China*

(Received 17 April 2023; accepted 25 August 2023; published 20 October 2023)

In inertial confinement fusion (ICF) implosions, mixing the ablator into the fuel and the hot spot is one of the most adverse factors that lead to ignition degradation. Recent experiments in the Marble campaign at the Omega laser facility and the National Ignition Facility demonstrate the significance of the temperature separation in heterogeneous mixing flows [Haines *et al.*, Nat. Commun. **11**, 544 (2020)]. In the present work we provide an approach to deal with thermally disequilibrium multicomponent flows with the ultimate aim to investigate the temperature separation impact on mixing and fusion burn. The present work is twofold: (a) We derive a model governing the multicomponent flows in thermal disequilibrium with transport terms and (b) we use the derived model to study the Rayleigh-Taylor (RT) instability in thermally relaxing multicomponent systems. The model is reduced from the full disequilibrium multiphase Baer-Nunziato model in the limit of small Knudsen number Kn $\ll 1$. Velocity disequilibrium is closed with the diffusion laws and only one mass-weighted velocity is retained formally. Thus, the complex wave structure of the original Baer-Nunziato model is simplified to a large extent and the obtained model is much more computationally affordable. Moreover, the capability to deal with finite-temperature relaxation is kept. Efficient numerical methods for solving the proposed model are also presented. Equipped with the proposed model and numerical methods, we further investigate the impact of thermal relaxation on the RT instability development at the ICF deceleration stage. On the basis of numerical simulations, we have found that for the RT instability at an interface between the high-density low-temperature component and the low-density high-temperature component, the thermal relaxation significantly suppresses the development of the instability.

DOI: 10.1103/PhysRevE.108.045108

I. INTRODUCTION

Mixing of the ablator into the fuel and the hot spot is considered to be one of the most adverse factors that leads to ignition degradation in inertial confinement fusion (ICF) implosions. Mixing takes place at different scales driven by different mechanisms. At the macroscopic scale where Kn $= \lambda/\Delta \ll 1$ (with λ and Δ being the mean free path and the characteristic spatial scale), the hydrodynamic instabilities [such as the Rayleigh-Taylor instability (RTI), Richtmyer-Meshkov instability, and Kelvin-Helmholtz instability] play predominate roles in causing mixing. With the continuous development of the hydrodynamic instabilities, the flows transition into turbulence where mixing happens at very different scales. At the small scale where Kn $= \mathcal{O}(1)$ the mass diffusion is proceeding all the time as result of random molecular motions (i.e., the kinetic effect). These two mechanisms have fundamental difference and scaling laws. For example, the mixing length caused by RTI and further induced turbulence can be scaled as $L_{\text{mix}} = \alpha A g t^2$, where α is a constant, A is the Atwood number, g is the acceleration, and t the time. In contrast, the mixing length caused by mass diffusion is expressed as $L_{\text{mix}} = \beta\sqrt{Dt}$, where D is the mass diffusivity and β is a constant. Recent works demonstrate that the mass. diffusion maybe the leading mixing mechanism for the implosion experiments under moderate temperature and convergence [1].

The ICF mixing is usually categorized into two types, i.e., atomic mixing and chunk mixing. In the former the mixing of the components takes place on the atomic scale, while in the latter the constituents are separated from each other as either at a rippled interface or in discrete clumps [2]. The ICF mixing is intrinsically heterogeneous as a combination of atomic mixing and nonatomic mixing. In the course of hydrodynamic development towards turbulence, the chunk mixing dominate the early stage and the atomic mixing takes over at later times. Meanwhile, the mass diffusion is always producing atomic mixing. From the perspective of numerical modeling, to discriminate different types of mixing with direct numerical simulation is a formidable task due to their very different characteristic scales. Therefore, one has to rely on mixing models that allow the coarse-grained description of the atomic mixing on an affordable grid (Fig. 1). The grid does not resolve the small scale mixing topology and the component mass fraction span over several computational cells in the macroscopic description. In the mixing cells some closure relation is needed to make the governing equations solvable. One of the most frequently used closures is temperature equilibrium, which is assumed in the ICF-relevant mixing models such as the k-L (k and L stands for the energy per unit mass and the characteristic

*Corresponding author: zhang_chao@iapcm.ac.cn; zhang-c@mail.ru
†Corresponding author: wang_lifeng@iapcm.ac.cn

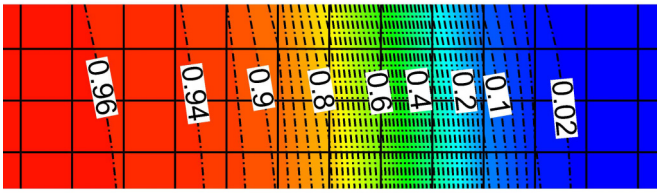

FIG. 1. The typical mass fraction distribution on the Eulerian grid in the case of heterogeneous mixing.

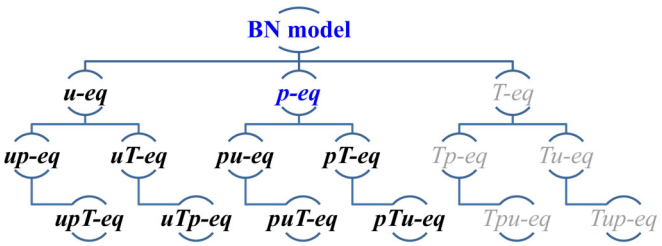

FIG. 2. The hierarchy of the reduced models of the Baer-Nunziato model.

dimension of the dominant eddies, respectively) model [3,4] and the BHR (named after families of the first three authors, i.e., Besnard-Harlow-Rauenzahn) model [5,6]. These models have been successfully used to simulate some experiments on the National Ignition Facility (NIF), e.g., see Refs. [7,8]. However, they mostly deal with planar experiments and struggle when applied to implosions. Moreover, they give numerical results that deviate from experimental measurements in the case of temperature separation. The root of such failure is attributed to the thermal equilibrium assumption, which has been proved in subsequent experiments at the Marble platform at NIF [9,10] (referred to as "Marble" henceforth).

As noted by Haines *et al.* [9,11], strong ion temperature separation arises during the shock flash as well as the compression heating of separated materials. Mechanisms that drive the component temperatures towards equilibrium include electron thermal conduction and local collision in atomic mixing. They happen in a timescale comparable to that of the ICF implosion (at least 1.6 ns for the Marble campaign on the Omega facility [11]). Thus, the ion temperatures of each species are not fully equilibrated in the course of ICF implosions. This means that in numerical simulation the components should have their own temperature in a mixing cell.

We aim to develop a multicomponent model to describe the temperature separation in mixing. Note that the phenomenlohgical two-field turbulence models [12–15] has the potential to deal with turbulence mixing with finite-temperature relaxation. However, here we adopt a more direct and strict derivation from a fully disequilibrium model—the BN model [16]. Due to the complexity and relaxation stiffness of the original BN model, a hierarchy of reduced models has been established (Fig. 2). Reduced models are derived in the limit of instantaneous relaxation of corresponding variable (chemical potential, pressure, velocity, and temperature). For example, in the case where the phase velocities relax instantaneously, one can derive the u-eq model via the asymptotic analysis. Starting from the u-eq model, one can further derive the up-eq model (i.e., the Kapila's five-equation model [17]) on the basis of the instantaneous phase pressure relaxation. Following such a procedure, a full hierarchy of reduced models can be obtained. A similar hierarchy has been described by Lund [18]; however, the velocity disequilibrium that is vital for modeling mass diffusion is neglected there.

The applicability of a particular reduced model is determined by the corresponding assumption on relaxation rates. In most applications the thermal relaxation time is smaller than the mechanical (pressure and velocity) relaxation times, and thus models in the right subsidiary are scarcely used. In term of the current work, we need a model that retains the thermal disequilibrium. Moreover, since mass diffusion is related to the species velocity difference, the velocity disequilibrium should also be maintained. Thus, the possible models to satisfy these requirements are the original BN model and the p-eq model. Here we focus on reformulation of the former by invoking the diffusion laws to close the velocity difference and abandoning the terms of order $\mathcal{O}(\mathrm{Kn}^2)$. Formally, the derived model has one velocity, i.e., the mass-weighted velocity. In fact, the hyperbolic subsystem of the model coincides with the six-equation model presented in Ref. [19], which is more robust than the Kapila's five-equation model in numerical implementation. This reduction significantly simplifies the wave structure of the hyperbolic subsystem of the model, thus improving the computational efficiency.

We propose second-order methods for solving the hyperbolic-parabolic-relaxation system. The numerical methods are validated against some benchmark problems. Being equipped with the model and numerical methods, we then investigate the RTI in the thermally relaxing multicomponent flows, especially the dependence of the mixing length on the thermal relaxation rate and the initial temperature separation.

The rest of the article is organized as follows. In Sec. II we derive the reduced temperature-disequilibrium model with diffusions. In Sec. III the numerical methods for solving the proposed model are briefly described. In Sec. IV some numerical results for validating the numerical methods are presented. Analysis of the RTI problem is performed in particular detail to investigate the impact of the thermal relaxation.

II. MODEL FORMULATION

A. The BN-type seven-equation model

The starting point of the following model formulation is the complete BN-type seven-equation model [16,20–22]. It reads

$$\frac{\partial \alpha_k \rho_k}{\partial t} + \nabla\cdot(\alpha_k \rho_k \boldsymbol{u}_k) = 0, \tag{1a}$$

$$\frac{\partial \alpha_k \rho_k \boldsymbol{u}_k}{\partial t} + \nabla\cdot(\alpha_k \rho_k \boldsymbol{u}_k \otimes \boldsymbol{u}_k - \alpha_k \overline{\overline{T}}_k) = -\overline{\overline{T}}_I\cdot\nabla\alpha_k + \mathcal{M}_k, \tag{1b}$$

$$\frac{\partial \alpha_k \rho_k E_k}{\partial t} + \nabla\cdot(\alpha_k \rho_k E_k \boldsymbol{u}_k - \alpha_k \overline{\overline{T}}_k\cdot\boldsymbol{u}_k) = -\boldsymbol{u}_I\cdot(\overline{\overline{T}}_I\cdot\nabla\alpha_k) + \boldsymbol{u}_I\mathcal{M}_k - p_I\mathcal{F}_k + \mathcal{Q}_k + q_k + \mathcal{I}_k, \tag{1c}$$

$$\frac{\partial \alpha_k}{\partial t} + \boldsymbol{u}_I\cdot\nabla\alpha_k = \mathcal{F}_k, \tag{1d}$$

where the notations used are standard: α_k, ρ_k, $\boldsymbol{u}_k$, p_k, $\overline{\overline{T}}_k$, and E_k are the volume fraction, phase density, velocity, pressure, stress tensor, and total energy of phase k.

The BN-type formulation can also be derived by averaging the one-phase governing equations [23–25]. Within such a framework the volume fraction α_k is the spatially average characteristic function X_k, which takes the value of 1 (or 0) in the presence (or absence) of the kth component, i.e.,

$$X_k(\boldsymbol{r},t)=\begin{cases}1, & \text{the point } \boldsymbol{r} \text{ in the material } k,\\ 0, & \text{otherwise.}\end{cases}$$

Then, we have

$$\alpha_k=\frac{1}{V}\int_V X_k dV=\frac{V_k}{V}.$$

The volume fraction α_k can be perceived as a macroscopic measure of spatial mixing extent when the microscopic interfaces cannot be accurately resolved. Moreover, the BN model can be used for describing both miscible and immiscible flows according to different interpretations of α_k and other variables [26].

For the sake of clarity we restrict our discussions within the scope of two-phase flows, $k=1,2$. The phase density ρ_k is defined as the mass per unit volume occupied by kth phase. The mixture density ρ is the sum of the partial densities $\alpha_k\rho_k$, i.e., $\rho=\sum\alpha_k\rho_k$. The last equation [Eq. (1d)] is written for only one component thanks to the saturation constraint for volume fractions $\sum_{k=1}^{2}\alpha_k=1$. The total energy is $E_k=e_k+\mathcal{K}_k$, where e_k and $\mathcal{K}_k=\frac{1}{2}\boldsymbol{u}_k\cdot\boldsymbol{u}_k$ are the internal energy and kinetic energy, respectively.

The variables with the subscript "I" represent the variables at interfaces, for which there are several possible definitions [20,22,27]. Here we choose the following:

$$\boldsymbol{u}_I=\boldsymbol{u}=\sum y_k\boldsymbol{u}_k,\quad p_I=\sum\alpha_k p_k,$$
$$\overline{\overline{\tau}}_I=\sum\alpha_k\overline{\overline{\tau}}_k,\quad \overline{\overline{T}}_I=-p_I\overline{\overline{I}}+\overline{\overline{\tau}}_I,$$

where y_k denotes the mass fraction $y_k=\alpha_k\rho_k/\rho$ and $\boldsymbol{u}$ is the mass-fraction-weighted mean velocity. Here we have used the mass-weighted velocity $\boldsymbol{u}$ to approximate the interface velocity $\boldsymbol{u}_I$. Other possible definitions for $\boldsymbol{u}_I$ as convex combination of component velocities will result in the same reduced model since $(\boldsymbol{u}_I-\boldsymbol{u})=\mathcal{O}(\mathrm{Kn})$, as to be shown in Sec. II C.

The interfacial stress $\overline{\overline{\tau}}_I$ is defined in such way that the thermodynamical laws are respected. In the present work we do not expand the issue on defining the interfacial variables since they are included in the terms of order Kn^2 that are to be omitted.

The interphase exchange terms include the velocity relaxation $\mathcal{M}_k$, the pressure relaxation $\mathcal{F}_k$, and the temperature relaxation $\mathcal{Q}_k$. They are as follows:

$$\begin{aligned}\mathcal{M}_k&=\vartheta(\boldsymbol{u}_{k^*}-\boldsymbol{u}_k),\\ \mathcal{F}_k&=\varsigma(p_k-p_{k^*}),\\ \mathcal{Q}_k&=\eta(T_{k^*}-T_k),\end{aligned}\tag{2}$$

where k^* denotes the conjugate component of the kth component, i.e., $k=1,\ k^*=2$ or $k=2,\ k^*=1$. The relaxation velocities are all positive $\vartheta>0,\ \eta>0,\ \varsigma>0$.

The phase stress tensor, $\overline{\overline{T}}_k$, can be written as

$$\overline{\overline{T}}_k=-p_k\overline{\overline{I}}+\overline{\overline{\tau}}_k.\tag{3}$$

For the viscous part we use the Newtonian approximation

$$\overline{\overline{\tau}}_k=2\mu_k\overline{\overline{D}}_k+\left(\mu_{b,k}-\tfrac{2}{3}\mu_k\right)\nabla\cdot\boldsymbol{u}_k,\tag{4}$$

where $\mu_k>0$ is the coefficient of shear viscosity and $\mu_{b,k}>0$ is the coefficient of bulk viscosity. The tensor $\overline{\overline{D}}_k$ is the deformation rate, which takes the following form:

$$\overline{\overline{D}}_k=\tfrac{1}{2}[\nabla\boldsymbol{u}_k+(\nabla\boldsymbol{u}_k)^T].$$

The heat conduction is represented by $q_k=\nabla\cdot(\lambda_k\nabla T_k)$. The term $\mathcal{I}_k$ is a volume energy source term, which can be used to model the laser energy absorption in direct drive ICF.

Performing straightforward calculus similar to that of Murrone [28], one can derive the following equation for the internal energy:

$$\begin{aligned}&\frac{\partial\alpha_k\rho_k e_k}{\partial t}+\nabla\cdot(\alpha_k\rho_k e_k\boldsymbol{u}_k)\\ &\quad=-\alpha_k p_k\nabla\cdot\boldsymbol{u}_k-p_I\mathcal{F}_k+(\boldsymbol{u}-\boldsymbol{u}_k)\cdot\mathcal{M}_k\\ &\qquad+(\boldsymbol{u}_k-\boldsymbol{u})\cdot(\overline{\overline{T}}_I\cdot\nabla\alpha_k)+\mathcal{G}_k,\end{aligned}\tag{5}$$

where $\mathcal{G}_k=q_k+\mathcal{I}_k+\mathcal{S}_k+\mathcal{Q}_k$.

$\mathcal{S}_k$ represents the friction heat,

$$\mathcal{S}_k=\nabla\cdot(\alpha_k\overline{\overline{\tau}}_k\cdot\boldsymbol{u}_k)-\boldsymbol{u}_k\cdot(\nabla\cdot\alpha_k\overline{\overline{\tau}}_k)=\alpha_k\overline{\overline{\tau}}_k:\overline{\overline{D}}_k.$$

B. Splitting diffusion-related terms

In continuum mechanics the mass diffusion strength is described through the difference between the phase velocity and the velocity of the mass center. We introduce the following definition of the diffusion velocity:

$$\boldsymbol{w}_k=\boldsymbol{u}_k-\boldsymbol{u}.\tag{6}$$

For future use, we gather the diffusion related terms separately. To do this, we replace $\boldsymbol{u}_k$ by $\boldsymbol{u}+\boldsymbol{w}_k$ to obtain the following reformulation of Eq. (1):

$$\frac{\partial\alpha_k\rho_k}{\partial t}+\nabla\cdot(\alpha_k\rho_k\boldsymbol{u})=-\nabla\cdot\boldsymbol{J}_k,\tag{7a}$$

$$\frac{\partial\alpha_k\rho_k\boldsymbol{u}}{\partial t}+\nabla\cdot(\alpha_k\rho_k\boldsymbol{u}\boldsymbol{u}-\alpha_k\overline{\overline{T}}_{ak})=-\overline{\overline{T}}_I\cdot\nabla\alpha_k+\mathcal{M}_k+\frac{\partial\alpha_k\rho_k\boldsymbol{w}_k}{\partial t}+\nabla\cdot(2\alpha_k\rho_k\boldsymbol{u}\boldsymbol{w}_k+\alpha_k\rho_k\boldsymbol{w}_k\boldsymbol{w}_k)+\nabla\cdot(\alpha_k\overline{\overline{T}}_{wk}),\tag{7b}$$

$$\frac{\partial \alpha_k \rho_k E_{ak}}{\partial t} + \nabla\cdot(\alpha_k \rho_k E_{ak}\boldsymbol{u} - \alpha_k \overline{\overline{T}}_{ak}\cdot\boldsymbol{u}) = -\boldsymbol{u}_I\cdot(\overline{\overline{T}}_I\cdot\nabla\alpha_k) + \boldsymbol{u}\mathcal{M}_k - p_I\mathcal{F}_k + \mathcal{Q}_k + q_k + \mathcal{I}_k - \frac{\partial \alpha_k \rho_k E_{wk}}{\partial t}$$
$$-\nabla\cdot[\alpha_k\rho_k(\boldsymbol{u}E_{wk} + E_{ak}\boldsymbol{w}_k + E_{wk}\boldsymbol{w}_k)]$$
$$+\nabla\cdot(\alpha_k\overline{\overline{T}}_{ak}\cdot\boldsymbol{w}_k + \alpha_k\overline{\overline{T}}_{wk}\cdot\boldsymbol{u} + \alpha_k\overline{\overline{T}}_{wk}\cdot\boldsymbol{w}_k), \tag{7c}$$

$$\frac{\partial \alpha_k}{\partial t} + \boldsymbol{u}\cdot\nabla\alpha_k = \mathcal{F}_k, \tag{7d}$$

where the diffusion flux

$$\boldsymbol{J}_k = \alpha_k\rho_k\boldsymbol{w}_k.$$

We have used the following decomposition:

$$E_k = E_{ak} + E_{wk}, \quad \overline{\overline{T}}_k = \overline{\overline{T}}_{ak} + \overline{\overline{\tau}}_{wk},$$

The quantities with subscript "*ak*" contain only the mass-centered velocity $\boldsymbol{u}$, i.e.,

$$E_{ak} = e_k + \tfrac{1}{2}\boldsymbol{u}\cdot\boldsymbol{u},$$
$$\overline{\overline{T}}_{ak} = -p_k\overline{\overline{I}} + \overline{\overline{\tau}}_{ak},$$
$$\overline{\overline{\tau}}_{ak} = 2\mu_k\overline{\overline{D}}_{ak} + \left(\mu_{b,k} - \tfrac{2}{3}\mu_k\right)\nabla\cdot\boldsymbol{u},$$
$$\overline{\overline{\tau}}_{wk} = 2\mu_k\overline{\overline{D}}_{wk} + \left(\mu_{b,k} - \tfrac{2}{3}\mu_k\right)\nabla\cdot\boldsymbol{w}_k$$
$$\overline{\overline{D}}_k = \overline{\overline{D}}_{ak} + \overline{\overline{D}}_{wk},$$
$$\overline{\overline{D}}_{ak} = \tfrac{1}{2}[\nabla\boldsymbol{u} + (\nabla\boldsymbol{u})^{\mathrm{T}}],$$
$$\overline{\overline{D}}_{wk} = \tfrac{1}{2}[\nabla\boldsymbol{w}_k + (\nabla\boldsymbol{w}_k)^{\mathrm{T}}].$$

The terms with $\boldsymbol{w}_k$ can be regarded as diffusion induced. Similarly, Eq. (5) can be reformulated as

$$\frac{\partial \alpha_k\rho_k e_k}{\partial t} + \nabla\cdot(\alpha_k\rho_k e_k\boldsymbol{u})$$
$$= -\alpha_k p_k\nabla\cdot\boldsymbol{u} - p_I\mathcal{F}_k + \boldsymbol{w}_k\cdot\mathcal{M}_k + \boldsymbol{w}_k\cdot(\overline{\overline{T}}_I\cdot\nabla\alpha_k)$$
$$- \nabla\cdot(\alpha_k\rho_k e_k\boldsymbol{w}_k) - \alpha_k p_k\nabla\cdot\boldsymbol{w}_k + \mathcal{G}_k. \tag{8}$$

C. Reduction of the BN model

Continuum assumption is usually accepted in the case of a small Knudsen number, i.e.,

$$\mathrm{Kn} = \frac{\lambda}{\Delta} \leqslant 0.001 \ll 1. \tag{9}$$

For moderate Mach number and collision of ions with comparable masses, it can be shown that [29]

$$\frac{|\boldsymbol{w}_k|}{u_{\mathrm{shock}}} \approx \frac{\lambda}{\Delta} \ll 1. \tag{10}$$

With such scale estimation, in the following we will drop the terms of order $\mathcal{O}(|\boldsymbol{w_k}^2|)$. The velocity relaxation $\mathcal{M}_k$ in the model (1) is related to the ion friction $\mu_{kk^*}\nu_i n_k(\boldsymbol{w}_k - \boldsymbol{w}_{k^*})$, where μ_{kk^*} is the reduced mass, ν_i is the ion collision frequency, and n_k is the number density. This term is finite under the concerned scenario. Thus, the velocity relaxation rate is estimated to be $\mathcal{O}(1)$. The general idea is to reduce the Baer-Nunziato model (1) via order analysis. More concretely, we will drop $\mathcal{O}(|\boldsymbol{w_k}^2|)$ terms and close $\mathcal{O}(|\boldsymbol{w_k}|)$ terms with the established diffusion laws.

The diffusion velocity is defined with the diffusion laws such as Fick's law, resulting in the redundance of the model (7b). Thus we can retain only one momentum equation, i.e., the sum of Eq. (7b),

$$\frac{\partial \rho\boldsymbol{u}}{\partial t} + \nabla\cdot\left(\rho\boldsymbol{u}\boldsymbol{u} - \sum\alpha_k\overline{\overline{T}}_{ak}\right) = \sum\nabla\cdot(\alpha_k\overline{\overline{T}}_{wk}). \tag{11}$$

With such evaluation, the equation for the internal energy [Eq. (8)] is reduced to

$$\frac{\partial \alpha_k\rho_k e_k}{\partial t} + \nabla\cdot(\alpha_k\rho_k e_k\boldsymbol{u})$$
$$= -\alpha_k p_k\nabla\cdot\boldsymbol{u} - p_I\mathcal{F}_k - \nabla\cdot(\alpha_k\rho_k e_k\boldsymbol{w}_k)$$
$$- \alpha_k p_k\nabla\cdot\boldsymbol{w}_k + \mathcal{G}_k. \tag{12}$$

By summing Eq. (7c) and abandoning terms of $\mathcal{O}(|\boldsymbol{w}_k|^2)$, one can obtain

$$\frac{\partial \rho E_a}{\partial t} + \nabla\cdot(\rho E_a\boldsymbol{u} - \overline{\overline{T}}_a\cdot\boldsymbol{u})$$
$$= \sum(\mathcal{Q}_k + q_k + \mathcal{I}_k) - \nabla\cdot\left(\sum\alpha_k\rho_k e_k\boldsymbol{w}_k\right)$$
$$+ \nabla\cdot\left(\sum\alpha_k\overline{\overline{T}}_{ak}\cdot\boldsymbol{w}_k + \sum\alpha_k\overline{\overline{T}}_{wk}\cdot\boldsymbol{u}\right), \tag{13}$$

where

$$E_a = \sum y_k E_{ak}.$$

Note that the enthalpy diffusion flux comes from the second and third terms on the right-hand side of Eq. (13).

After the above reduction we can have the following closed system consisting of the phase mass equations (7a), the mixture momentum equation (11), the phase internal energy equation (12), and the volume fraction equation (1d). For clarity, we present the obtained model as follows:

$$\frac{\partial \alpha_k\rho_k}{\partial t} + \nabla\cdot(\alpha_k\rho_k\boldsymbol{u}) = \underbrace{-\nabla\cdot\boldsymbol{J}_k}_{\text{Mass Diff.}}, \tag{14a}$$

$$\frac{\partial \rho\boldsymbol{u}}{\partial t} + \nabla\cdot(\rho\boldsymbol{u}\boldsymbol{u}) = \underbrace{\nabla\cdot\left(\sum\alpha_k\overline{\overline{T}}_k\right)}_{\text{Visc.}}, \tag{14b}$$

$$\frac{\partial \alpha_k\rho_k e_k}{\partial t} + \nabla\cdot(\alpha_k\rho_k e_k\boldsymbol{u}) + \alpha_k p_k\nabla\cdot\boldsymbol{u}$$
$$= \underbrace{-p_I\mathcal{F}_k}_{\text{Pres. Relax}} \underbrace{-\nabla\cdot(\alpha_k\rho_k e_k\boldsymbol{w}_k) - \alpha_k p_k\nabla\cdot\boldsymbol{w}_k}_{\text{Mass Diff.}}$$
$$+ \underbrace{\mathcal{S}_k}_{\text{Visc.}} + \underbrace{\mathcal{Q}_k}_{\text{Temp. Relax}} + \underbrace{q_k + I_k}_{\text{Heat Cond. and Heat Scr.}}, \tag{14c}$$

$$\frac{\partial \alpha_k}{\partial t} + \boldsymbol{u}\cdot\nabla\alpha_k = \underbrace{\mathcal{F}_k}_{\text{Pres. Relax}}. \tag{14d}$$

The absence of a mass diffusion term in the volume fraction equation (14d) is due to the particular choice of interfacial velocity $\boldsymbol{u}_I = \boldsymbol{u}$. In a more general case we can reformulate Eq. (1d) as follows:

$$\frac{\partial \alpha_k}{\partial t} + \boldsymbol{u}\cdot\nabla\alpha_k = (\boldsymbol{u} - \boldsymbol{u}_I)\cdot\nabla\alpha_k + \mathcal{F}_k.$$

Here one can see that the first term on the right-hand side is actually of order $\mathcal{O}(\mathrm{Kn}^2)$ as long as the $\boldsymbol{u}_I$ is of the same order as $\boldsymbol{u}_k$. This means that even in this general situation Eq. (14d) holds in the context our approximation.

In the framework of the fractional step method, the hydrodynamic subsystem of Eq. (14) is nonconservative due to the equation for internal energy and the volume fraction. To alleviate the nonconservativeness, we use the mixture energy equation (13) as an auxiliary equation in solving the hyperbolic subsystem as the six-equation model [19]. An instantaneous pressure relaxation follow after solving the hyperbolic subsystem, thus resulting in a pressure-equilibrium model. Such an approach ensures robustness in numerical implementation with marginal sacrifice of computation efficiency.

In comparison with the hydrodynamic model in Refs. [30,31], the proposed model additionally resolves the intrinsic density ρ_k and the component specific internal energy e_k. Note that the standard model like that in Refs. [30,31] only provides the partial density $\widehat{\rho}_k = \alpha_k\rho_k$ and the mixture internal energy e. This allows our model to compute the temperatures of each component. The mixture energy equation (13) is formally consistent with those in Refs. [30,31]. The main difference consists in the constitutive law for the viscous stress. In our formulation the component velocity is determined with the average velocity $\boldsymbol{u}$ (that is provided by the model) and the diffusion velocity $\boldsymbol{w}_k$ (which is provided by the diffusion law), and thus the viscous stress of each component can be determined.

Note that Eq. (13) is not a strict consequence of Eq. (14) since the latter loses a momentum equation after reduction. However, Eq. (13) is only invoked in solving the hyperbolic part where the consistency remains.

The proposed model provides a first step towards the inclusion of the ion temperature separation effect in macroscopic radiation-hydrodynamics simulations. In comparison with the closure framework proposed in Ref. [32], the ion disequilibrium is kept while the ion-electron temperature equilibrium is assumed. The latter is valid when the concerned characteristic timescale is much larger than the ion-electron relaxation time.

However, the ion-electron temperature disequilibrium is also important for ICF applications whose characteristic timescale is comparable to the ion-electron temperature relaxation time. A strategy to consider such effect is to simplify the multifluid plasma model by performing the Chapman-Enskog-like asymptotic expansion under the assumption that some relaxation timescales are small parameters. Such a method is strict; however, it is also very complicated. A much simpler phenomenological method is to neglect the mass and momentum of electron and treat it as an external field to the ions. Moreover, the extension to the case with three or more components does not pose fundamental difficulty as long as the derivation starts from a symmetrical formulation of the BN type model. In the present work we do not dig into these complexities and concentrate on the fundamental step that allows the ion temperature separation.

We now check the entropy dissipative property of the model. The full entropy equation before reduction can be derived in a way similarly as in Refs. [28,33], which read

$$\alpha_k\rho_k T_k\frac{D_k s_k}{Dt} = (p_k - p_I)\mathcal{F}_k + \mathcal{G}_k + p_k\boldsymbol{w}_k\cdot\nabla\alpha_k + \boldsymbol{w}_k\cdot\overline{\overline{T}}_I\cdot\nabla\alpha_k + (\boldsymbol{u} - \boldsymbol{u}_k)\cdot\mathcal{M}_k. \tag{15}$$

The last three terms are evaluated to be of $\mathcal{O}(\mathrm{Kn}^2)$ and therefore abandoned. Thus, the entropy equation is reduced to the following:

$$\alpha_k\rho_k T_k\frac{D_k s_k}{Dt} = (p_k - p_I)\mathcal{F}_k + \mathcal{G}_k. \tag{16}$$

The model (14) keeps the equations for the internal energy, and abandoning a momentum equation has no impact on the entropy equation. Therefore, the above reduced entropy equation can also be derived from the reduced model (14). With [Eq. (16)], one can readily prove the entropy inequality in the absence of external heat flux and energy source,

$$\sum_{k=1}^{2}\alpha_k\rho_k\frac{D_k s_k}{Dt} + \sum_{k=1}^{2}\nabla\cdot\left(\frac{\boldsymbol{q}_k}{T_k}\right) - \sum_{k=1}^{2}\frac{\mathcal{I}_k}{T_k} \geqslant 0. \tag{17}$$

The proof can be performed in a manner similar to that in our previous paper [33], and we provide a brief proof in the Appendix.

In the model (14) all the mass diffusion effects are gathered into the terms containing $\boldsymbol{w}_k$. In comparision with the model in the literature [31], our model contains the mass diffusion contribution to the viscous stress. Moreover, as the original Baer-Nunziato model, this model includes all the disequilibrium effects in phase pressure and temperature, which is driven towards equilibrium with the corresponding relaxation terms.

The derived model has certain advantages over the widely used model of Cook [31] in the following aspects: (a) It retains the pressure-temperature disequilibria between phases through the relaxation terms, thus allowing us to consider the disequilibrium effects between components. Such disequilibrium is significant in some phenomena of plasma physics. (b) It frees the hydrodynamic step of the temperature equilibrium constraint, which is the root of spurious oscillations for diffuse interface problems [34]. Some special numerical cures exist in the literature [35,36]. (c) As to the constitutive law for viscous stress, the viscous stress of each component is determined with their own velocity (derived by virture of the diffusion law), which is compatible with thermodynamic relations. In the model of Cook [31], only the mass-weighted velocity is used for the evaluation of viscous stress, which is decoupled from the diffusion effect. These two approaches may lead to noticeable difference in simulation. A numerical test is to be considered in Sec. IV to demonstrate this issue.

D. Diffusion models

To make the model solvable, some closure relations are needed to relate the diffusion terms to basic variables

(including density, temperature, and pressure). The diffusion coefficients are usually derived from kinetic theories or from experimental measurements. For ordinary neural flows without plasma, there are some well-accepted equations to describe the diffusion processes, for example, Fourier's law for heat flux, Newton's law for viscous stress, and Fick's law for mass diffusion. However, for plasma flows, the diffusion laws are far more complicated. The electron-ion disequilibrium may also play an important role. For simplicity, in the present paper we concentrate on the case of electron-ion equilibrium and show the feasibility of our approach to consider multicomponent plasma flows with diffusions. This assumption should not limit the present model's applicability to the disequilibrium ion-electron temperature flows. Further work on the ion-electron disequilibrium plasma flows will follow in our next work. Moreover, one can also regard our model as the limit of instantaneous ion-electron relaxation time of some ion-electron temperature disequilibrium model.

Based on the above discussions, we use the ion-electron equilibrium Spitzer-Harm model [37] for the heat flux. The commonly used models to calculate the plasma viscosity and mass diffusion include Clerouin's model [38] for viscosity and Paquette's model [39] for mass diffusion, respectively. In recent years, driven by the need to evaluate species mixing or separation in thermonuclear inertial confinement fusion plasmas, a series of transport models [30,40,41] for multicomponent plasmas are derived. In these models the mass diffusion is driven by the gradients of field variables such as species concentration, ion or electron pressure (barodiffusion) and ion or electron temperature (thermal diffusion). For Simakov [30], the closure law for the diffusion velocity is written as follows:

$$\boldsymbol{w}_k = -\sum D_{kj}\boldsymbol{d}_j + D_k^T \nabla(\ln T_i), \tag{18}$$

and

$$\boldsymbol{d}_k = \nabla x_k + (x_k - y_k)\nabla(\ln p) + (z_k - y_k)\frac{\nabla p_e}{p} + \left(\frac{Z_k n_k}{n_e} - \frac{Z_k^2 n_k}{\sum_j Z_j^2 n_j}\right)\frac{n_e}{n}\frac{\beta_0 \nabla T_e}{T}, \tag{19}$$

where x_k, y_k, z_k, Z_k, and n_k are the number fraction, the mass fraction, the charge fraction, the charge number, and the number density of component k, respectively. D_{kj} and D_k^T are the generalized diffusion coefficient and the thermodiffusion coefficient, respectively. They depend on the collision frequency, thermal speed, and ion charge. The parameter β_0 is a function of effective charge number. For more details see Ref. [30]. In the present work we only consider the diffusion driven by gradients of concentration and pressure and neglect the thermodiffusion.

In the case of two components, the above representation is identical to that of Kagan and Tang [29]:

$$\boldsymbol{w}_k = -\frac{D}{y_k}(\nabla y_k + D_{pk}\nabla \log p), \tag{20}$$

where we have omitted the electro- and thermodiffusions. The barodiffusion coefficient D_{pk} is determined as follows:

$$D_{pk} = y_k y_{k*}(M_{k*} - M_k)\left(\frac{y_1}{M_1} + \frac{y_2}{M_2}\right). \tag{21}$$

where M_k is the ion mass of the k component.

III. NUMERICAL METHOD

The model (14) is solved by using the splitting procedure. According to physical processes, the model is split into six subsystems, i.e., the hyperbolic subsystem, the viscous subsystem, the pressure relaxation subsystem, the temperature relaxation subsystem, the heat conduction subsystem, and the mass diffusion subsystem. These subsystems are solved within each time step in order. The solution of one subsystem serves as the initial condition for the next.

Note that these physical processes are in fact coupled with each other; the splitting procedure is a merely numerical solution strategy. However, direct splitting may neglect some coupling mechanisms. For example, here we assume that the pressure relaxation happens instantaneously in comparison with the thermal process and mass diffusion. This means that the pressure equilibrium should be maintained during the temperature relaxation, heat conduction, and mass diffusion. Such pressure equilibrium can be ensured by splitting the pressure relaxation, i.e.,

$$\mathcal{F}_k = \mathcal{F}_k^0 + \mathcal{F}_k^{\mathrm{tr}} + \mathcal{F}_k^{\mathrm{hc}} + \mathcal{F}_k^{\mathrm{md}},$$

where $\mathcal{F}_k^0$ represents the instantaneous pressure relaxation before the thermal processes and mass diffusion. $\mathcal{F}_k^{\mathrm{tr}}$, $\mathcal{F}_k^{\mathrm{hc}}$, and $\mathcal{F}_k^{\mathrm{md}}$ are the pressure relaxation during the temperature relaxation, heat conduction, and mass diffusion, respectively. In other words, $\mathcal{F}_k^0$ drives the component pressures into an initial equilibrium, while $\mathcal{F}_k^{\mathrm{tr}}$, $\mathcal{F}_k^{\mathrm{hc}}$, and $\mathcal{F}_k^{\mathrm{md}}$ maintain the pressure equilibrium by enforcing $\frac{\partial p_1}{\partial t} = \frac{\partial p_2}{\partial t}$ during each splitting process. In fact, the latter three terms can be determined explicitly by invoking the equilibrium of pressure variation rates.

In the following subsections we present the numerical methods for each split subsystem.

A. Hyperbolic subsystem

The split hyperbolic subsystem coincides with the six-equation model proposed in Refs. [17,19]. It reads as follows:

$$\frac{\partial \alpha_k \rho_k}{\partial t} + \nabla\cdot(\alpha_k \rho_k \boldsymbol{u}) = 0, \tag{22a}$$

$$\frac{\partial \rho \boldsymbol{u}}{\partial t} + \nabla\cdot(\rho \boldsymbol{u}\boldsymbol{u}) = 0, \tag{22b}$$

$$\frac{\partial \alpha_k \rho_k e_k}{\partial t} + \nabla\cdot(\alpha_k \rho_k e_k \boldsymbol{u}) + \alpha_k p_k \nabla\cdot\boldsymbol{u} = 0, \tag{22c}$$

$$\frac{\partial \alpha_k}{\partial t} + \boldsymbol{u}\cdot\nabla\alpha_k = 0. \tag{22d}$$

The numerical methods for the hyperbolic and parabolic parts are similar to those described in our previous works [33].

As shown in Ref. [17], the wave speeds for this split model in 1D is $\lambda_{\mathrm{hyper}} = c_{\mathrm{mix}} \pm u$, u(of multiplicity 4) with $c_{\mathrm{mix}}^2 =$

$\sum y_k c_k^2$. Thus the stable time step required is

$$\Delta t < \Delta t_{\text{hyper}} = \text{CFL}\frac{\Delta x}{\max(\lambda_{\text{hyper}})},$$

where the CFL number is taken to be 0.2 if not mentioned.

This subsystem is solved in the framework of finite-volume method. The numerical flux is computed with the HLLC Riemann solver [19]. For high-order extension we reconstruct $[\alpha_k\rho_k,\ u,\ p_k,\ \alpha_k]$ with the fifth-order MLP scheme [42]. This reconstruction strategy has been proven to be free of spurious oscillations in temperature [33]. For time integration, we implement the Heun method.

B. Viscous subsystem

The viscous subsystem can be written as follows:

$$\frac{\partial \alpha_k\rho_k}{\partial t} = 0, \tag{23a}$$

$$\frac{\partial \rho \boldsymbol{u}}{\partial t} = \nabla\cdot\Big(\sum \alpha_k \overline{\overline{\tau}}_{ak}\Big) + \nabla\cdot\Big(\sum \alpha_k \overline{\overline{\tau}}_{wk}\Big), \tag{23b}$$

$$\frac{\partial \alpha_k\rho_k e_k}{\partial t} = \alpha_k \overline{\overline{\tau}}_k : \overline{\overline{D}}_k, \tag{23c}$$

$$\frac{\partial \alpha_k}{\partial t} = 0. \tag{23d}$$

By observing the mass equations, we see that the partial masses remain constant at this stage, as does the mixture density and mass fraction. If we assume a constant diffusivity for Fick's law, then one can deduce that $\boldsymbol{w}_k$ and $\overline{\overline{\tau}}_{wk}$ are both constants. This make the numerical solution of the momentum equation as simple as that of the standard model [31], only with an additional constant being included. The explicit scheme requires the following stable time step

$$\Delta t < \Delta t_{\text{vis}} = \frac{\Delta x^2}{\frac{8}{3}\max\left(\frac{\mu}{\rho}\right)}, \quad \mu = \sum \alpha_k \mu_k.$$

In more general case, the diffusion velocity $\boldsymbol{w}_k$ depends on temperature and pressure. To account for this nonlinearity, a simple iteration procedure is performed.

Note that $\mathcal{O}(|\boldsymbol{w}_k|^2)$ terms are kept in the internal energy equation to ensure the positivity of the right-hand side term.

C. Pressure relaxation subsystem

The split pressure relaxation subsystem reads

$$\frac{\partial \alpha_k\rho_k}{\partial t} = 0, \tag{24a}$$

$$\frac{\partial \rho \boldsymbol{u}}{\partial t} = 0, \tag{24b}$$

$$\frac{\partial \alpha_k\rho_k e_k}{\partial t} = -p_I \mathcal{F}_k^0, \tag{24c}$$

$$\frac{\partial \alpha_k}{\partial t} = \mathcal{F}_k^0. \tag{24d}$$

To solve this stiff ODE system with pressure relaxation rate $\varsigma \to \infty$, we have recently proposed an efficient fixed point iteration method in Ref. [43]. This iteration method performs a convex average of the component pressures, ensuring fast convergence and pressure positivity. The proposed relaxation method has been applied to the case with three components. For further details, please see Ref. [43].

D. Temperature relaxation subsystem

Here we describe some details for the solution of the thermal relaxation subsystem, which reads

$$\frac{\partial \alpha_k\rho_k}{\partial t} = 0, \tag{25a}$$

$$\frac{\partial \rho \boldsymbol{u}}{\partial t} = 0, \tag{25b}$$

$$\frac{\partial \alpha_k\rho_k e_k}{\partial t} = \mathcal{Q}_k - p_I \mathcal{F}_k^{\text{tr}}, \tag{25c}$$

$$\frac{\partial \alpha_k}{\partial t} = \mathcal{F}_k^{\text{tr}}. \tag{25d}$$

To account for the interface motion due to arising pressure disequilibrium, we adopt the following assumption

$$\frac{\partial \alpha_k}{\partial t} = \mathcal{F}_k^{\text{tr}} := \Lambda \mathcal{Q}_k \tag{26}$$

where the exchanged energy $\mathcal{Q}_k = \eta(T_{k^*} - T_k)$ and the interfacial pressure is approximated as $p_I = \sum \alpha_k p_k$.

The volume fraction varies in such a way that the phasic pressure equilibrium is maintained, implicitly meaning that the pressure relaxation rate is much larger than the thermal relaxation rate. By using the pressure equilibrium condition

$$\frac{\partial p_1}{\partial t} = \frac{\partial p_2}{\partial t},$$

one can derive the evolution equation for α_k in the case of polytropic gas EOS as follows:

$$\Lambda = \frac{1}{p_I + \frac{\sum p_k/\alpha_k}{\sum(\gamma_k - 1)/\alpha_k}}. \tag{27}$$

Note that partial densities and momentum remain unchanged during the thermal relaxation stage. Reformulation of Eqs. (25)–(27) gives

$$\frac{\partial T_k}{\partial t} = \widehat{\eta}_k(T_{k^*} - T_k), \tag{28}$$

where

$$\widehat{\eta}_k = \frac{\frac{\sum p_k/\alpha_k}{\sum(\gamma_k-1)/\alpha_k}}{\left[\frac{\sum p_k/\alpha_k}{\sum(\gamma_k-1)/\alpha_k} + p_I\right] m_k C_{vk}}\eta.$$

For the solution of the nonlinear equations (26) and (28), iterative methods should be used, where for each iteration one solves the following linearized ODEs in each time step Δt

$$\frac{\partial T_k^{(s+1)}}{\partial t} = \widehat{\eta}_k^{(s)}\left[T_{k^*}^{(s+1)} - T_k^{(s+1)}\right], \tag{29}$$

where (s) denotes the iteration index. The analytical solution for the above ODEs are as follows:

$$T_1^{(s+1)} = A + B\widehat{\eta}_1^{(s)}, \quad T_2^{(s+1)} = A - B\widehat{\eta}_2^{(s)}$$

$$A = \frac{T_{10}\widehat{\eta}_2^{(s)} + T_{20}\widehat{\eta}_1^{(s)}}{\widehat{\eta}_2^{(s)} + \widehat{\eta}_1^{(s)}}, \quad B = \frac{(T_{10} - T_{20})C}{\widehat{\eta}_2^{(s)} + \widehat{\eta}_1^{(s)}},$$

$$C = e^{-[\widehat{\eta}_1^{(s)} + \widehat{\eta}_2^{(s)}]\Delta t},$$

where T_{10} and T_{20} are the initial component temperature at the beginning of the temperature relaxation stage.

The iterations are performed until the convergence condition $|T_k^{(s+1)} - T_k^{(s)}| < \epsilon$ is satisfied. Acceleration of the temperature relaxation with the Newton's method is also possible; however, one has to deal with the complexity and nonsmoothness of the dependency of η on T_k.

E. Heat conduction subsystem

The subsystem governs heat conduction reads

$$\frac{\partial \alpha_k \rho_k}{\partial t} = 0, \tag{30a}$$

$$\frac{\partial \rho \boldsymbol{u}}{\partial t} = 0, \tag{30b}$$

$$\frac{\partial \alpha_k \rho_k e_k}{\partial t} = q_k + I_k - p_I \mathcal{F}_k^{\mathrm{hc}}, \tag{30c}$$

$$\frac{\partial \alpha_k}{\partial t} = \mathcal{F}_k^{\mathrm{hc}}. \tag{30d}$$

The term $\mathcal{F}_k^{\mathrm{hc}}$ can be determined in totally similar way in determining $\mathcal{F}_k^{\mathrm{tr}}$. In fact, simply by replacing $\mathcal{Q}_k$ in Sec. III D with $(q_k + I_k)$, one can obtain the expression for $\mathcal{F}_k^{\mathrm{hc}}$, i.e.,

$$\frac{\partial \alpha_k}{\partial t} = \mathcal{F}_k^{\mathrm{hc}} = \Lambda(q_k + I_k). \tag{31}$$

For multicomponent heat conduction, we implement the implicit scheme proposed in Ref. [21].

F. Mass diffusion subsystem

The subsystem for mass diffusion reads:

$$\frac{\partial \alpha_k \rho_k}{\partial t} = -\nabla \cdot \boldsymbol{J}_k, \tag{32a}$$

$$\frac{\partial \rho \boldsymbol{u}}{\partial t} = 0, \tag{32b}$$

$$\frac{\partial \alpha_k \rho_k e_k}{\partial t} = -\nabla \cdot (\alpha_k \rho_k e_k \boldsymbol{w}_k) - \alpha_k p_k \nabla \cdot \boldsymbol{w}_k - p_I \mathcal{F}_k^{\mathrm{md}}, \tag{32c}$$

$$\frac{\partial \alpha_k}{\partial t} = \mathcal{F}_k^{\mathrm{md}}. \tag{32d}$$

For clarity, we introduce the following definitions:

$$\mathcal{C}_k := -\nabla \cdot (\alpha_k \rho_k \boldsymbol{w}_k),$$
$$\mathcal{E}_k := -\alpha_k \rho_k \boldsymbol{w}_k \cdot \nabla e_k - \alpha_k p_k \nabla \cdot \boldsymbol{w}_k.$$

In comparison with the temperature relaxation subsystem, the additional complexity here consists in the variation of the partial mass $\alpha_k \rho_k$; however, the derivation procedure is totally similar to that for defining $\mathcal{F}_k^{\mathrm{tr}}$ in Sec. III D. The derived equation describing the volume fraction variation under the pressure equilibrium takes the following form:

$$\frac{\partial \alpha_1}{\partial t} = \mathcal{F}_k^{\mathrm{md}} = \frac{\left(\frac{G_1 \mathcal{E}_1}{\alpha_1} - \frac{G_2 \mathcal{E}_2}{\alpha_2}\right) + \left(\frac{p_1 \mathcal{C}_1}{\alpha_1 \rho_1} - \frac{p_2 \mathcal{C}_2}{\alpha_2 \rho_2}\right)}{\left(\frac{G_1}{\alpha_1} + \frac{G_2}{\alpha_2}\right) p_I + \left(\frac{p_1}{\alpha_1} + \frac{p_2}{\alpha_2}\right)}, \tag{33}$$

where $G_k = \gamma_k - 1$.

Note that the diffusion term in Eq. (33) is to maintain the obtained pressure equilibrium. This does not contradicts Eq. (14d), but is a result of the sequence in solving the split subsystems. A similar numerical strategy is adopted in solving phase transition problems [44].

At this stage the mixture mass is conserved. In numerical solution, one may solve only one diffusion equation for partial density, while the remaining partial density is derived by subtracting one partial density from the mixture density.

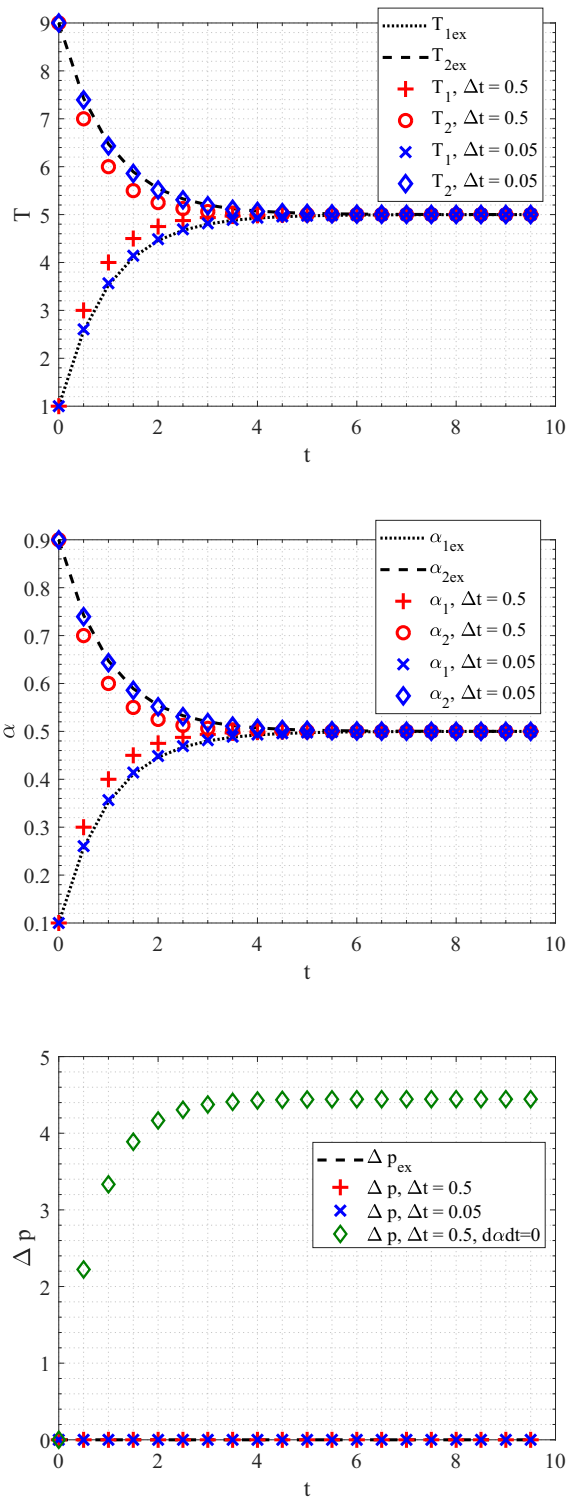

FIG. 3. The numerical results for the pure temperature relaxation problem. Top: component temperatures; middle: volume fractions; bottom: the pressure disequilibrium, measured as $\Delta p = |p_1 - p_2|$.

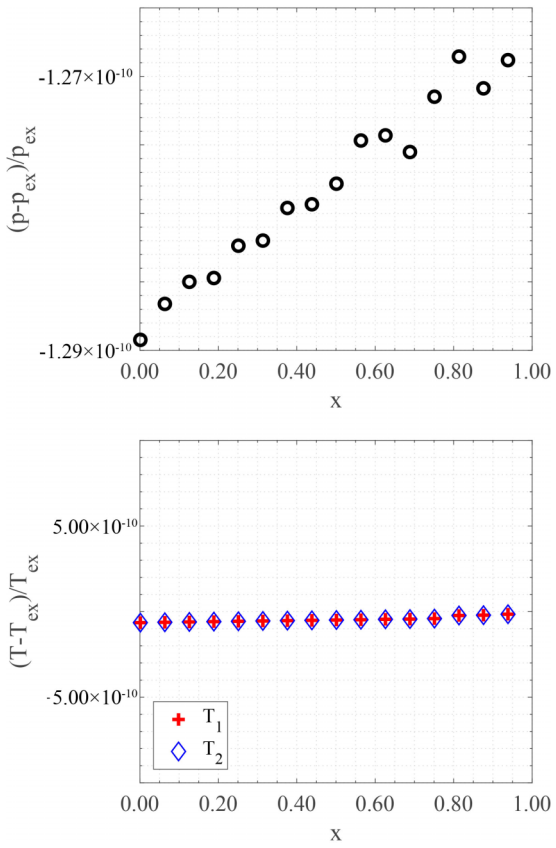

FIG. 4. The relative error of pressure and temperature for the pure advection problem.

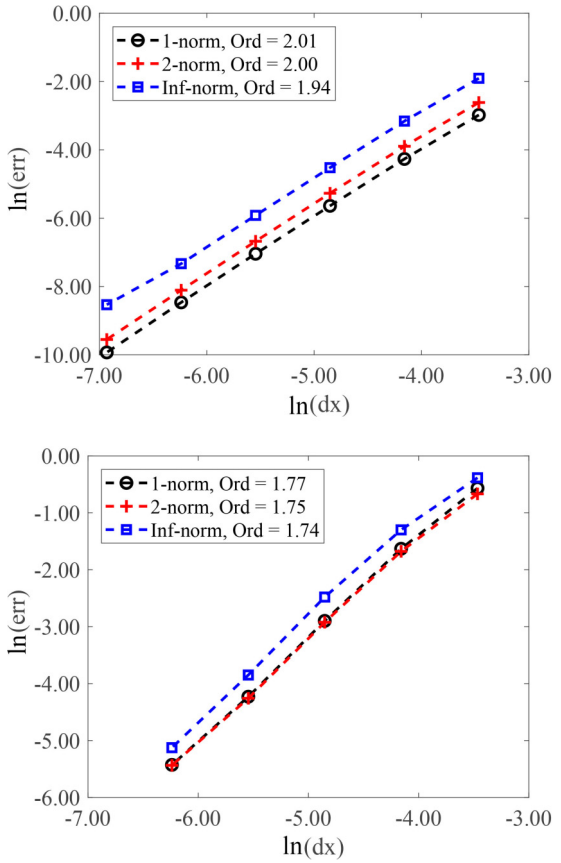

FIG. 5. The convergence rate for the mass diffusion problem. Upper: the pure diffusion problem; lower: the advection-diffusion problem.

The involved spatial derivatives are approximated with the central difference scheme. With Fick's law, the mass diffusion equation takes the following form:

$$\rho \frac{\partial y_1}{\partial t} = \nabla \cdot (\rho D \nabla y_1).$$

The stable time step required by this diffusion equation is

$$\Delta t < \Delta t_{\mathrm{D}} = \frac{\rho \Delta x^2}{2 \max(D)}.$$

The overall time step is determined as the minimum of these stable time steps, i.e., $\Delta t = \min[\Delta t_{\mathrm{hyper}},\ \Delta t_{\mathrm{vis}},\ \Delta t_D]$.

IV. NUMERICAL RESULTS

In this section we present some numerical results to validate the proposed model and numerical methods. Moreover, with the aid of the proposed method we investigate the impact of thermal relaxation on RT instability development.

A. The temperature relaxation

Assume that a computational cell contains two materials with different initial temperatures, we only consider the temperature relaxation between them without the hydrodynamics. The two materials are characterized by $\gamma_1 = 1.4$, $Cv_1 = \frac{1}{4}$ and $\gamma_2 = 1.4$, $Cv_2 = \frac{1}{8}$, respectively. The relaxation rates are assumed to be $\widehat{\eta}_1 = \widehat{\eta}_2 = 5$ and $\Lambda\eta = \frac{1}{2}$. The initial states is assigned to be $[\alpha_1\rho_1,\ \alpha_2\rho_2,\ \rho u,\ T_1,\ T_2,\ \alpha_1]^0 = [1,\ 2,\ 0,\ 1,\ 9,\ 0.1]$. Such a setting is compatible with Eqs. (27) and (28). The corresponding analytical solution for temperatures $T_1 = 5 - 5\exp(-t)$ and $T_2 = 5 + 5\exp(-t)$. The numerical results for temperatures, volume fractions, and the pressure difference are displayed in Fig. 3. One can see that with the decrease of the time step, the numerical results tend to converge to the exact solution.

Moreover, our method well maintains the pressure equilibrium ($\Delta p = |p_1 - p_2| \approx 0$) during the temperature relaxation, as displayed in Fig. 4. In comparison, if we do not consider the corresponding variation of the volume fraction (i.e., $\frac{\partial \alpha}{\partial t} = 0$), then the pressure equilibrium is violated, as demonstrated in the bottom subfigure of Fig. 3.

B. The mass diffusion problem

1. The pure diffusion problem

Let us consider a pure diffusion problem as in Refs. [45,46]. The two components are characterized by the polytropic EOS with the adiabatic coefficients $\gamma_1 = 2.0$ and $\gamma_2 = 1.4$ and densities $\rho_1 = 20.0$ and $\rho_2 = 1.0$, respectively. In the computational domain [0,1] the fluids are initially in temperature and pressure equilibrium which means $(\gamma_k - 1)\rho_k C_{vk} = \text{const}$. This relation gives a constraint for prescribing the heat capacities C_{vk}.

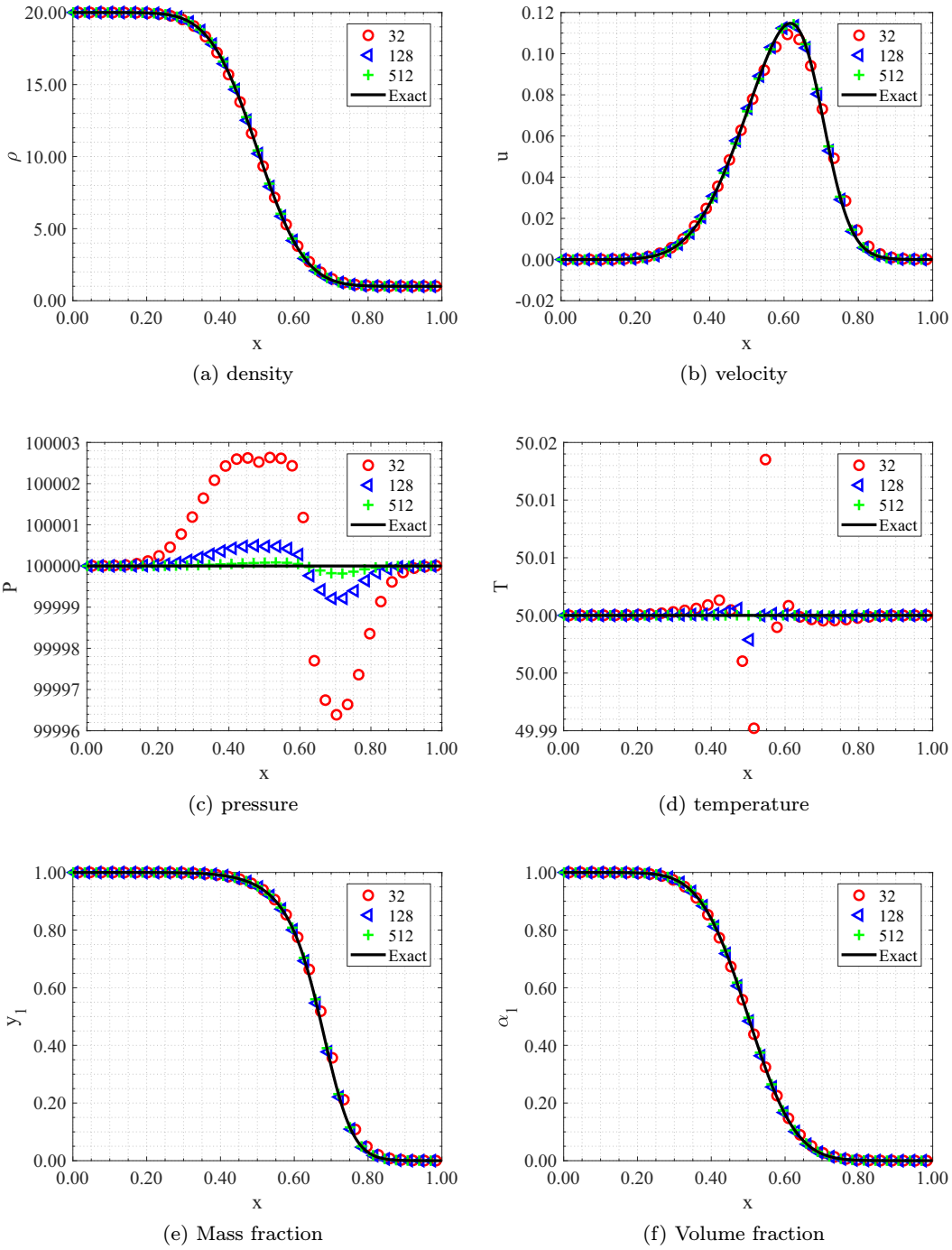

FIG. 6. The numerical results in the pure diffusion problem for density, velocity, pressure, temperature, mass fraction, and volume fraction with the refinement of grid.

The initial mixture density and partial density are given as follows:

$$\rho = \tfrac{1}{2}(\rho_1 + \rho_2) - \tfrac{1}{2}(\rho_1 - \rho_2)\mathrm{erf}(z),$$
$$\rho y_1 = \tfrac{1}{2}\rho_1 - \tfrac{1}{2}\rho_1 \mathrm{erf}(z), \tag{34}$$

where

$$z = \frac{x - x_0}{\sqrt{4Dt + h_0^2}}.$$

In the present test we use $t = 0.0$, $x_0 = 0.5$, and $h_0 = 0.02$ for prescribing the initial condition. Here Fick's law and a constant diffusivity $D = 0.01$ are assumed.

With the pressure as large as $p = 1 \times 10^5$, the Mach number is so small that the compressibility effect can be neglected. In this case, given the mixture density profile, one can derive the mass-weighted mean velocity,

$$u = -\frac{D}{\rho}\frac{\partial \rho}{\partial x}.$$

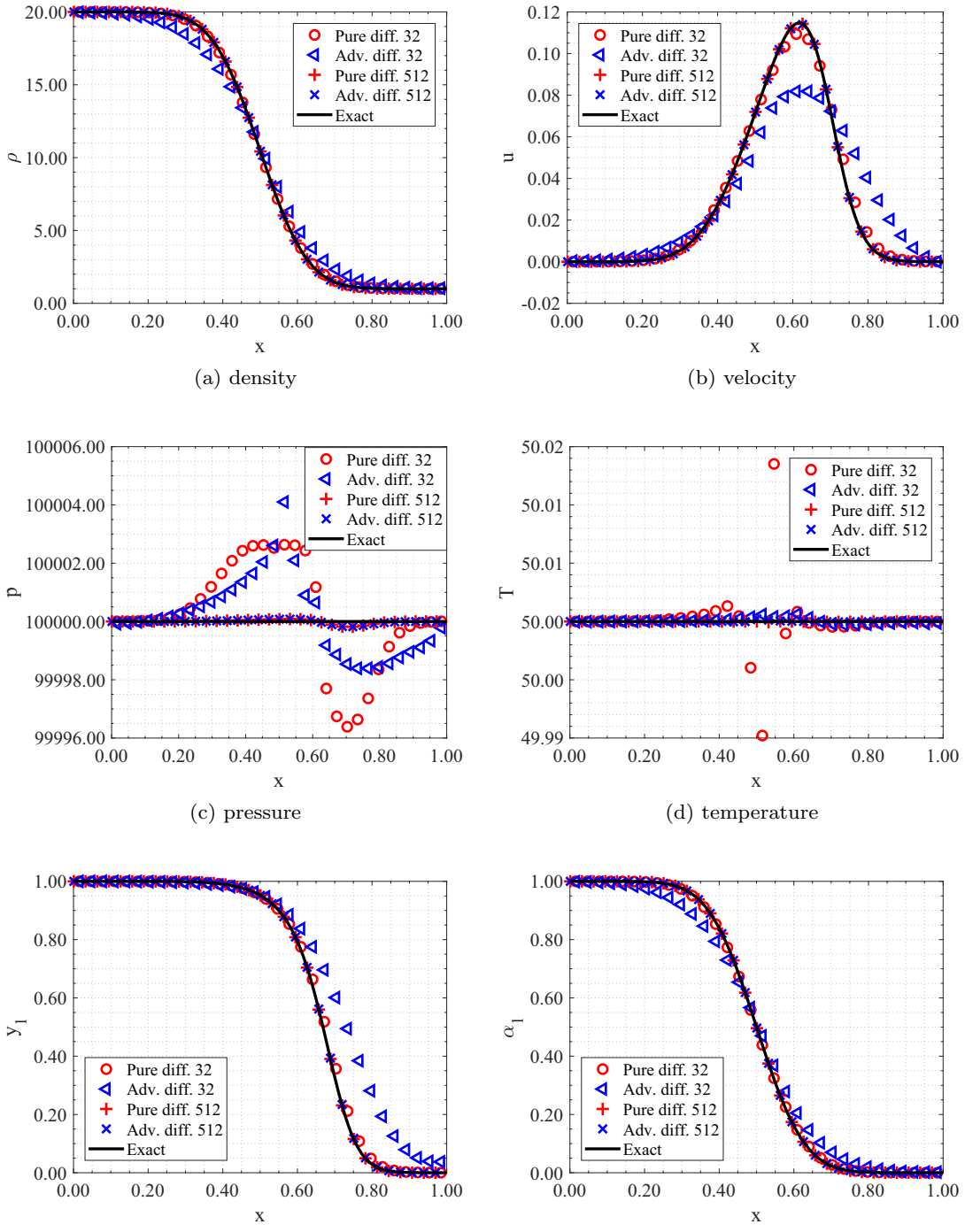

FIG. 7. The numerical results in the pure-diffusion and advection-diffusion problems for density, velocity, pressure, temperature, mass fraction, and volume fraction.

Moreover, the analytical solution for density to this pure diffusion problem is given by Eq. (34) [45,47].

Computations are performed to the time moment $t = 0.5$ on a series of refining grids of 32, 64, 128, 256, 512, and 1024 cells. Reflective boundary conditions are imposed on both sides. The errors for density are defined as its distance to the analytical solution Eq. (34). The convergence performance is displayed in Fig. 5. One can see that the second order is reached as expected. The corresponding convergence performance for different variables are demonstrated in Fig. 6.

2. The pure advection problem

We here verify that the model and corresponding numerical methods maintain the P-T equilibrium. The initial condition within [0,1] is the same as the last test and is mirrored into [1,2]. The periodic boundary conditions are imposed on both

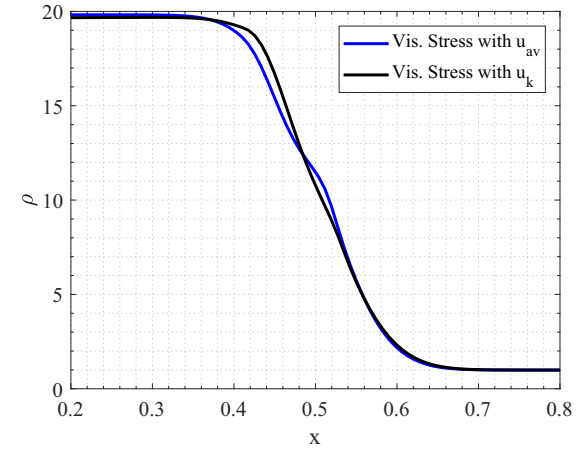

(a) Density

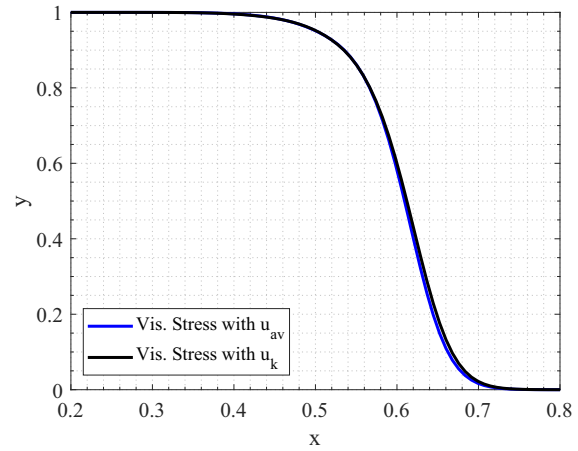

(b) Mass fraction

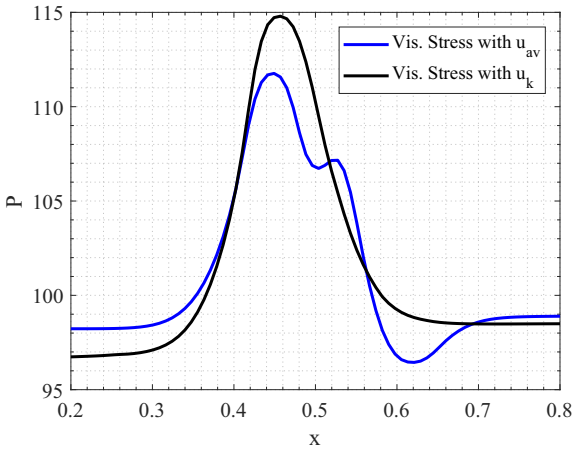

(c) Pressure

FIG. 8. The numerical results for the mass diffusion problem with viscous effect. "Vis. stress with u_k/u_{av}": numerical results obtained with the viscous stress being calculated with the component velocity and the mass-weighted velocity.

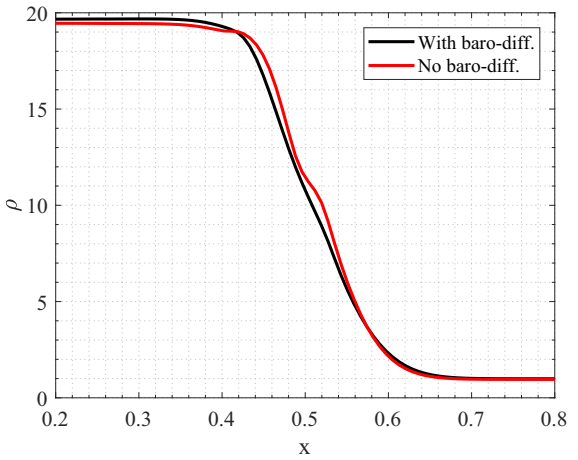

(a) Density

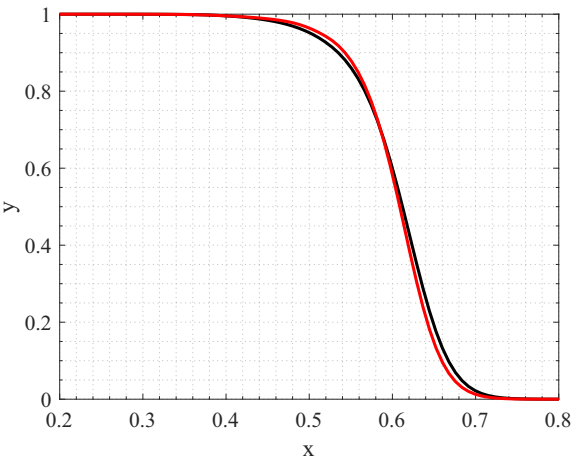

(b) Mass fraction

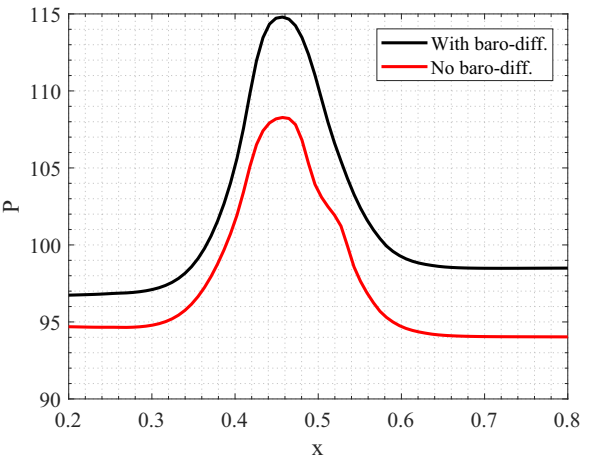

(c) Pressure

FIG. 9. The numerical results for the mass diffusion problem with or without the barodiffusion effect.

sides. The mixture is advected rightwards with a uniform velocity $u = 4$. At the time moment $t = 0.5$ the pressure error and the temperature error are as small as 10^{-10} (Fig. 4), which means that the P-T equilibrium is well maintained to the error level 10^{-10}.

3. The advection-diffusion problem

We continue to consider the advection-diffusion problem where the multicomponent fluid is transported by a uniform velocity $u = 4.0$ while diffusing. By choosing a reference

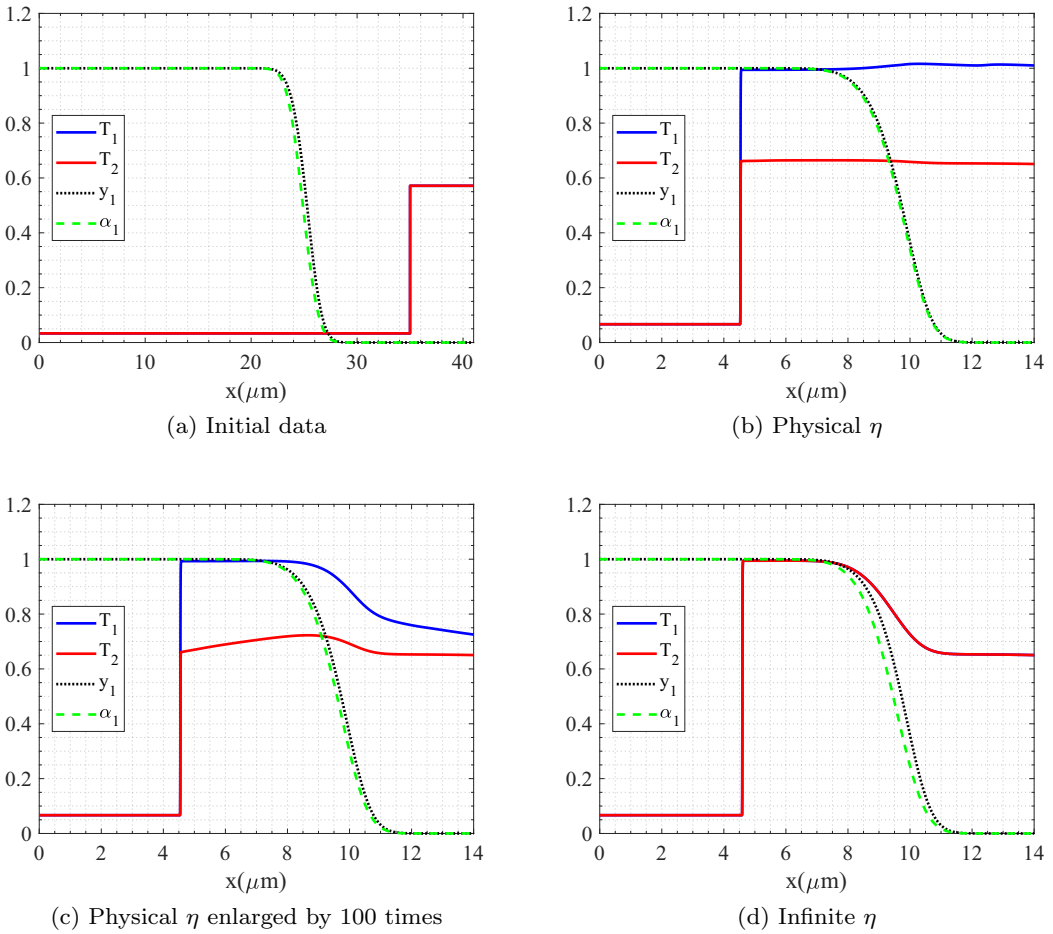

(a) Initial data (b) Physical η

(c) Physical η enlarged by 100 times (d) Infinite η

FIG. 10. The variable (component temperatures, the volume fraction, and the mass fraction) distributions after the shock travels through the mixing zone. Nondimensional temperatures displayed are $T_k/(1500\ \mathrm{MK})$. (a) The initial profile, (b) the numerical results at $t = 6 \times 10^{-3}$ ns with physical relaxation rate η_{Phys}, (c) the numerical results with $100\eta_{\mathrm{Phys}}$, and (d) the numerical results with $\eta \to \infty$.

moving at the transport velocity, one can see that the analytical solution is still described by Eq. (34), only with a transported interface center. The computational domain is enlarged to [0,4] and the interface center is transported to $x = 2.5$ at $t = 0.5$. Similarly, we obtain the convergence rate for this problem as displayed in Fig. 5. The convergence rate is somewhat smaller than that for the pure diffusion problem since the numerical resolution of the advection part adds to some error.

The comparison between the pure-diffusion and advection-diffusion problems are displayed in Fig. 7. One can observe that on the coarse grid the numerical results (for the density, velocity, and mass-volume fraction) of the advection-diffusion problem suffer from more deviations from the exact solutions. This can be explained by the fact that extra numerical dissipation is needed in solving the advection part. On the other hand, the introduced numerical dissipation also smooths the pressure-temperature oscillations, as can be seen in Figs. 7(c) and 7(d).

4. The barodiffusion and viscous effect

The initial density and velocity profiles are the same as those in the pure-diffusion problem in Sec. IV B. To show the ability of our method to deal with the barodiffusion and viscous effect, we consider a problem with considerable compressibility effect under the background pressure $p = 100$. Under such pressure the compressibility results in a nonuniform pressure profile, i.e., nonzero pressure gradient. Thus, the barodiffusion begins to effect the results. The kinetic viscosity is taken to be $\nu = 50D$, which is large enough to show the impact of the viscous dissipation. Initial and boundary conditions are the same as the test in Sec. IV B.

As for the viscous part, the conventional way is to determine the viscous stress by using the mass-weighted velocity as in Ref. [31]. Different from this approach, we use the component velocity to calculate their respective viscous stress. The numerical results obtained by these two approaches are compared in Fig. 8. One can see noticeable difference between these numerical results, especially in pressure. A new extreme arises in the pressure profile obtained with the u_{av} approach. The difference in pressure results in the corresponding difference in density.

We continue to consider the diffusion law with the barodiffusion being included, i.e., Eq. (20). Let us assume that the two components are carbon (C) and deuterium (D), respectively. According to Eq. (21), the barodiffusion coefficient for carbon is negative ($D_{p1} < 0$) and that for the deuterium is

positive ($D_{p2} > 0$). As can be seen from Fig. 9, in the neighborhood of the diffuse front, the pressure gradient is along $-x$. Thus, for carbon the barodiffusion flux $-\rho D D_{p1} \nabla \log p < 0$, which is opposite the mass fraction gradient driven flux $-\rho D \nabla y_1 > 0$. Therefore, in Fig. 9, one can observe that the carbon mass fraction is less diffused with the barodiffusion effect being included.

C. The shock passage through a mixing zone

In this test we demonstrate the capability of the proposed model (14) to deal with temperature separation phenomenon when the shock travels through the mixing zone. The mixture consists of two polytropic components with adiabatic coefficients $\gamma = 2.0$ and $\gamma = 5/3$. The heat capacity is calculated by $C_v = N_0 k_b (1 + Z)/(\gamma A)$, where N_0 is the Avogadro constant, k_b is the Boltzmann constant, A and Z are the atomic weight and number, respectively. Again, we assume that the two components are carbon ($A = 12$ g/mol, $Z = 6$) and deuterium ($A = 2$ g/mol, $Z = 1$).

The one-dimensional computational domain is of length $L = 40.96$ μm. The initial mixture density is characterized by Eq. (34) with $x_0 = 0.6L$, $h_0 = L/10$, and $D = 0.02$ cm^2/μs. A leftward shock of Mach number 5 hits the mixing interface. The temperature disequilibrium in the initial postshock zone is neglected since the concentration of the second component is negligibly small ($y_2 = 1 \times 10^{-6}$). Moreover, such assumption is justified by Eq. (28), the relaxation rate approaches infinity when the partial mass $m_k \to 0$.

The preshock mixture is in temperature and pressure equilibrium with uniform profile $p = 5000$ Mbar and $T = 100$ MK. The component densities can be determined as $\rho_1 = 2.0617$ g/cm^3 and $\rho_2 = 1.2027$ g/cm^3 via the EOSs. The postshock mixture density, pressure, and velocity are determined with the Rankie-Hugonoit relation of the first component. With the mass fraction y_2 being given, the equilibrium temperature in the postshock zone can be calculated via the pressure-temperature equilibrium relations [32,48].

The initial profiles for the component temperatures, volume fraction, and mass fraction are demonstrated in Fig. 10(a). We first perform computation with the physical temperature relaxation rate determined with the Coloumb collosion frequency [49]. At time $t = 6 \times 10^{-3}$ ns the shock travels through the mixing interface, and temperature disequilibrium arises in the postshock zone [Fig. 10(b)]. The temperature difference can be as large as 525 MK. The slight divergence in temperatures in the postshock zone is due to the pressure relaxation mechanism.

We then increase the physical temperature relaxation rate by 100 times and perform the same computation. The corresponding results are displayed in Fig. 10(c). It can be observed that the temperature disequilibrium is obviously reduced.

For comparison we also present the numerical results with the temperature equilibrium model (or $\eta \to \infty$) in Fig. 10(d). The equilibrium temperature lies between the component temperatures in Figs. 10(b) and 10(c). The deviation between the mass fraction and the volume fraction is more obvious in Fig. 10(d). This is because the temperature relaxation leads to the variation of the volume fraction while it has no impact on the mass fraction, as analyzed in Sec. III D. Comparison between the temperature-equilibrium and the temperature-disequilibrium model indicates that the commonly used temperature-equilibrium model may be inadequate for evaluating the temperature relaxation effect in mixing topology evolution.

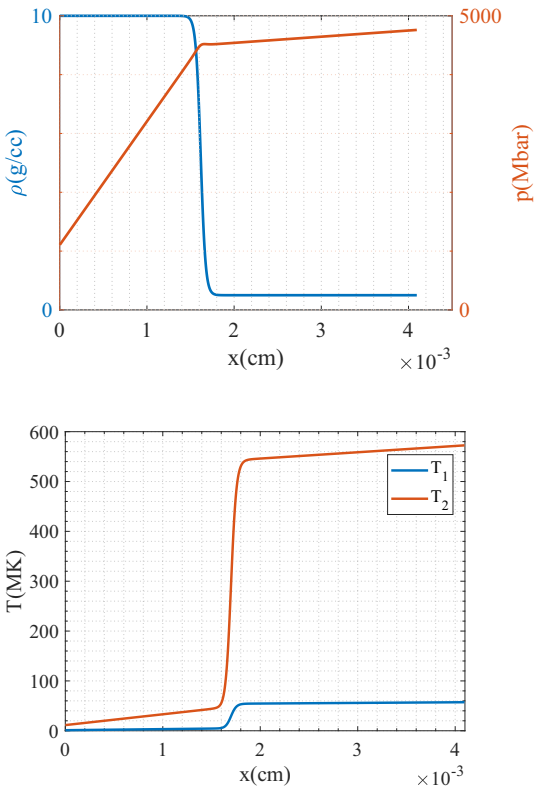

FIG. 11. The initial condition for the RT instability problem. Top: mixture density and pressure; bottom: component temperature. The mixture density $\rho = \sum \alpha_k \rho_k$.

D. The RT instability problem under thermal relaxation

In this section we consider a planar RT instability problem in a computational domain $(x, y) \in [0\ \mu\text{m}, 10.24\ \mu\text{m}] \times [0\ \mu\text{m}, 40.96\ \mu\text{m}]$. The initial condition along $y = L_y/2 = 5.12$ cm is demonstrated in Fig. 11. The acceleration is set to be 2.1×10^5 cm/μs^2, which is equal to that of a realistic implosion during the deceleration stage on the Omega facility [50]. The temperature at the interface zone is also within the temperature range in ICF implosion.

Note that we assume a smeared interface, which maybe a result of various mixing mechanisms such as molecular diffusion or turbulence. The mixing interface center is perturbed with a cosine profile $x_0 = 0.4L_x - 0.03L_y \cos(2\pi y/L_y)$. Inside the smeared interface the component temperatures relax towards a equilibrium one. Such thermal relaxation mechanism has a significant impact on the RT instability development, which is shown below by the following direct simulations. The relaxation rate is determined with the formula in the NRL plasma formulary [49].

To ensure grid independence, we first compare the numerical results obtained on a series of refining grids from 320×80 cells to 2560×640 cells. The corresponding results

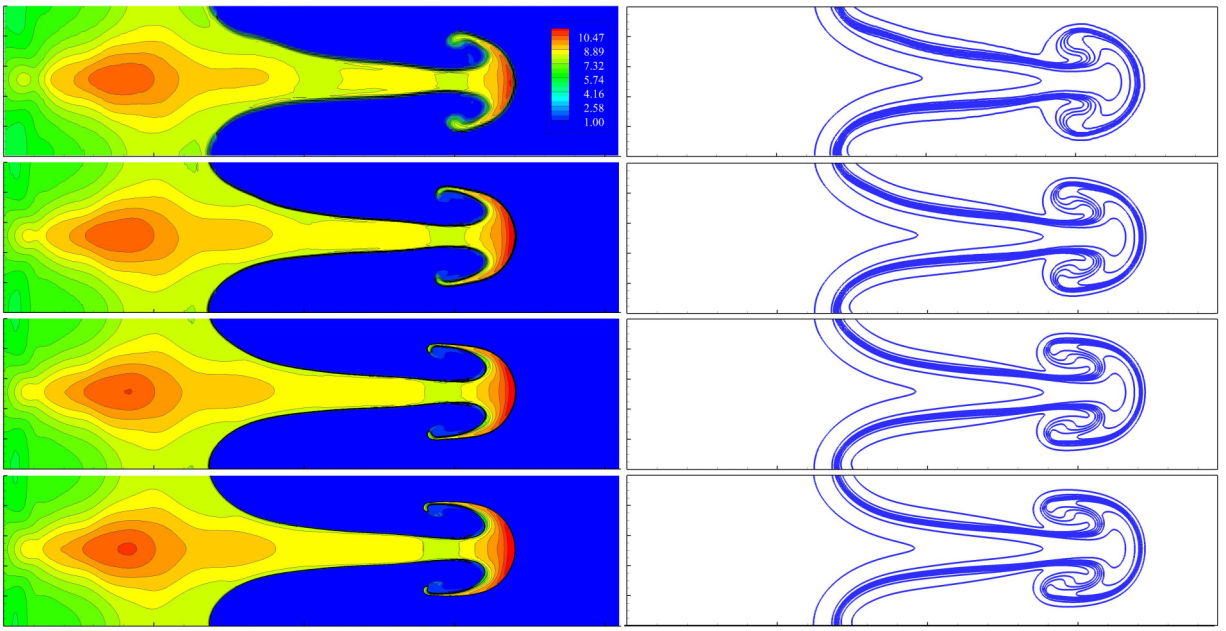

FIG. 12. The distribution of the mixture density ρ (left) and mass fraction y_1 (right) on series of refining grids (From top to bottom: 320×80, 640×160, 1280×320, 2560×640). Ten uniform contours from 0.01 to 0.99 for y_1 are displayed on the right.

are displayed in Fig. 12. One can see that the numerical results tend to converge with physical diffusions being included. The mixing length evolution with time displayed in Fig. 14 also confirms the convergence.

Then we investigate the sensitivity of the mixing length evolution to the relaxation rate η on the 1280×320 grid. The relaxation rate η is taken to be 1×10^5, 1×10^6, and ∞. The case $\eta = \infty$ corresponds to the case where component temperatures relax instantaneously, i.e., temperature equilibrium.

The density and mass fraction distributions at 0.2 ns with different relaxation rates are shown in Fig. 13. The evolution of the mixing length (bubble-to-spike distance) with time is demonstrated in Fig. 14. It can be seen that the thermal relaxation tend to suppress the growth of the mixing length. The main mechanism here lies in the unsteady acceleration of the interface caused by the thermal relaxation. The details of the physical mechanism will be dealt with in a separate paper and here we focus on the model itself.

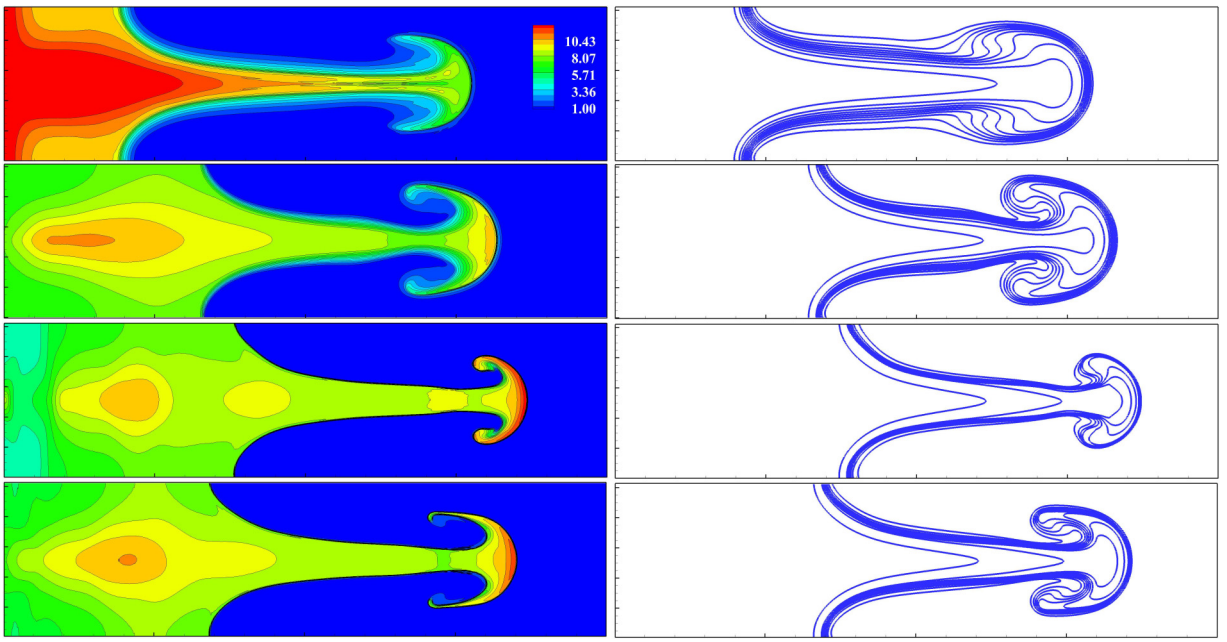

FIG. 13. The distribution of the mixture density ρ (left) and mass fraction y_1 (right) with different relaxation rates η at the time moment $t = 0.2$ ns. From top to bottom: $\eta = 0$, 1×10^6, ∞, and η determined by physical model (last row). Ten uniform contours from 0.01 to 0.99 for y_1 are display on the right.

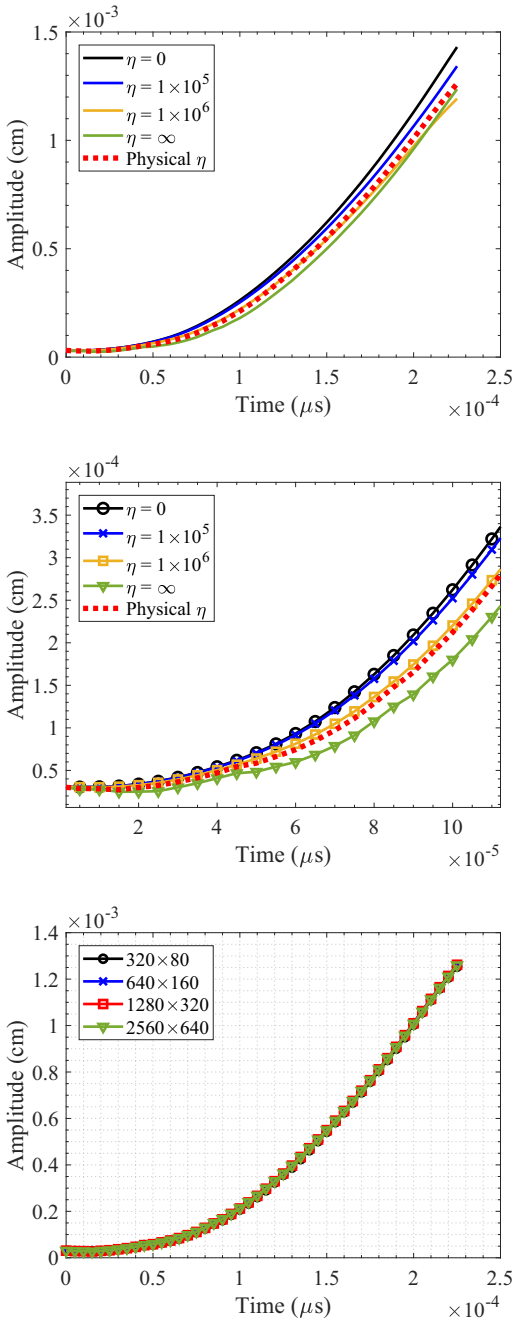

FIG. 14. The evolution of the mixing length with time. Top and middle subfigures are the results corresponding to different relaxation rates η. The bottom subfigure shows the grid independence of the numerical results.

Based on the simulation results, we can see that under the ICF deceleration condition the temperature equilibrium or disequilibrium assumptions lead to underestimation or overestimation of the mixing length evolution. The temperature relaxation timescale is comparable to the ICF-concerned timescale, and the temperature separation is diminishing at a finite rate. This effect should be considered for the accurate evaluation of the mixing in ICF.

V. CONCLUSION

In the present paper we have presented a temperature disequilibrium diffuse-interface model for compressible multicomponent flows with interphase heat transfer and diffusions (including viscous, heat conduction, and mass diffusion). The model is reduced from the BN model in the limit of small Knudsen number (Kn $\ll 1$) and consists of six equations including phase density equations, mixture momentum equation, phase internal energy equations, and the volume fraction equation. Velocity difference is closed by the mass diffusion laws, and thus the velocity of each component is available. The viscous stress is determined by component velocities rather than mixture velocity in the literature. Moreover, the model has included the effect of finite thermal relaxation. We have described second-order numerical methods for solving the advection-diffusion part of the proposed model. As for the thermal relaxation, we propose method to keep the pressure equilibrium. Being equipped with this model and its solution methods, we have considered an RT instability problem under the ICF deceleration condition with a finite thermal relaxation rate. We have performed a parametric study on the dependence of the mixing length development on the relaxation rate. Direct numerical simulations demonstrate that for the RT instability at an interface between the high-density low-temperature component and the low-density high-temperature component, the thermal relaxation tend to suppress the development of the instability. Further details of this mechanism will appear in our future papers.

ACKNOWLEDGMENT

The present study is supported by National Natural Science Foundation of China (Grants No. 12205022 and No. 11975053).

C.Z. conceptualized the work, derived the model, designed numerical methods, wrote the code, analyzed the results and wrote the original draft. L.W. supervised the project, formulated the problem statement, analyzed the results and reviewed the manuscript.

APPENDIX

Here we provide the proof of the entropy inequality Eq. (17). Inserting the pressure relaxation Eq. (2) into Eq. (17) and performing some reformulations, one obtains

$$\alpha_1\rho_1\frac{D_1 s_1}{Dt}+\alpha_2\rho_2\frac{D_2 s_2}{Dt}+\nabla\cdot\left(\frac{\boldsymbol{q}_1}{T_1}\right)+\nabla\cdot\left(\frac{\boldsymbol{q}_2}{T_2}\right)-\frac{\mathcal{I}_1}{T_1}-\frac{\mathcal{I}_2}{T_2}$$
$$=\frac{\alpha_2\varsigma(p_1-p_2)^2}{T_1}+\frac{\alpha_1\varsigma(p_2-p_1)^2}{T_2}+\frac{\eta(T_2-T_1)^2}{T_1T_2}$$
$$+\frac{\mathcal{S}_1}{T_1}+\frac{\mathcal{S}_2}{T_2}+\boldsymbol{q}_1\cdot\nabla\left(\frac{1}{T_1}\right)+\boldsymbol{q}_2\cdot\nabla\left(\frac{1}{T_2}\right). \tag{A1}$$

The first three terms on the right-hand side are obviously non-negative. The term $\mathcal{S}_k=\alpha_k\overline{\overline{\tau}}_k:\overline{\overline{D}}_k$ represents the kinetic energy dissipation due to viscous friction and is non-negative as long as the viscosity coefficient $\mu_k\geqslant 0$. The non-negativity

of the terms $\boldsymbol{q}_k \cdot \nabla(\frac{1}{T_k})$ are ensured by Fourier's law $\boldsymbol{q}_k = -\alpha_k \lambda_k \nabla T_k$. Thus entropy does not decrease in the absence of external heat flux and energy source, which does not contradict the second law of thermodynamics.

[1] A. B. Zylstra, N. M. Hoffman, H. W. Herrmann, M. J. Schmitt, Y. H. Kim, K. Meaney, A. Leatherland, S. Gales, C. Forrest, V. Yu. Glebov *et al.*, Diffusion-dominated mixing in moderate convergence implosions, Phys. Rev. E **97**, 061201(R) (2018).

[2] D. C. Wilson, P. S. Ebey, T. C. Sangster, W. T. Shmayda, V. Yu. Glebov, and R. A. Lerche, Atomic mix in directly driven inertial confinement implosions, Phys. Plasmas **18**, 112707 (2011).

[3] G. Dimonte and R. Tipton, K-l turbulence model for the self-similar growth of the Rayleigh-Taylor and Richtmyer-Meshkov instabilities, Phys. Fluids **18**, 085101 (2006).

[4] O. Schilling, Self-similar reynolds-averaged mechanical–scalar turbulence models for Rayleigh-Taylor, Richtmyer-Meshkov, and Kelvin-Helmholtz instability-induced mixing in the small atwood number limit, Phys. Fluids **33**, 085129 (2021).

[5] D. Besnard, F. H. Harlow, R. M. Rauenzahn, and C. Zemach, Turbulence transport equations for variable-density turbulence and their relationship to two-field models, Report No. LAUR-12303, Los Alamos National Lab., Los Alamos, NM, USA (1992), https://www.osti.gov/biblio/7271399.

[6] F. F. Grinstein, J. A. Saenz, and M. Germano, Coarse grained simulations of shock-driven turbulent material mixing, Phys. Fluids **33**, 035131 (2021).

[7] V. A. Smalyuk, D. T. Casey, D. S. Clark, M. J. Edwards, S. W. Haan, A. Hamza, D. E. Hoover, W. W. Hsing, O. Hurricane, J. D. Kilkenny *et al.*, First measurements of hydrodynamic instability growth in indirectly driven implosions at ignition-relevant conditions on the national ignition facility, Phys. Rev. Lett. **112**, 185003 (2014).

[8] B. J. Albright, T. J. Murphy, B. M. Haines, M. R. Douglas, J. H. Cooley, T. H. Day, N. A. Denissen, C. Di Stefano, P. Donovan, S. L. Edwards *et al.*, Experimental quantification of the impact of heterogeneous mix on thermonuclear burn, Phys. Plasmas **29**, 022702 (2022).

[9] R. E. Olson, T. J. Murphy, B. M. Haines, M. R. Douglas, B. J. Albright, M. A. Gunderson, Y. Kim, T. Cardenas, C. E. Hamilton, and R. B. Randolph, Development of the marble experimental platform at the national ignition facility, Phys. Plasmas **27**, 102703 (2020).

[10] T. J. Murphy, B. J. Albright, M. R. Douglas, T. Cardenas, J. H. Cooley, T. H. Day, N. A. Denissen, R. A. Gore, M. A. Gunderson, J. R. Haack *et al.*, Results from single-shock marble experiments studying thermonuclear burn in the presence of heterogeneous mix on the national ignition facility, High Energy Density Phys. **38**, 100929 (2021).

[11] B. M. Haines, R. C. Shah, J. M. Smidt, and B. J. Abright, Observation of persistent species temperature separation in inertial confinement fusion mixtures, Nat. Commun. **11**, 544 (2020).

[12] A. Llor, *Statistical Hydrodynamic Models for Developed Mixing Instability Flows: Analytical" 0D" Evaluation Criteria, and Comparison of Single-and Two-Phase Flow Approaches* (Springer Science & Business Media, New York, 2005), Vol. 681.

[13] A. Llor and P. Bailly, A new turbulent two-field concept for modeling Rayleigh-Taylor, Richtmyer-Meshkov, and Kelvin-Helmholtz mixing layers, Laser Part. Beams **21**, 311 (2003).

[14] D. L. Youngs, Numerical simulation of mixing by Rayleigh-Taylor and Richtmyer-Meshkov instabilities, Laser Part. Beams **12**, 725 (1994).

[15] R. Saurel, G. Huber, G. Jourdan, E. Lapébie, and L. Munier, Modelling spherical explosions with turbulent mixing and post-detonation, Phys. Fluids **24**, 115101 (2012).

[16] M. R. Baer and J. W. Nunziato, A two-phase mixture theory for the deflagration-to-detonation transition (DDT) in reactive granular materials, Int. J. Multiphase Flow **12**, 861 (1986).

[17] A. K. Kapila, R. Menikoff, J. B. Bdzil, S. F. Son, and D. S. Stewart, Two-phase modeling of deflagration-to-detonation transition in granular materials: Reduced equations, Phys. Fluids **13**, 3002 (2001).

[18] H. Lund, A hierarchy of relaxation models for two-phase flow, SIAM J. Appl. Math. **72**, 1713 (2012).

[19] R. Saurel, F. Petitpas, and R. Berry, Simple and efficient relaxation methods for interfaces separating compressible fluids, cavitating flows and shocks in multiphase mixtures, J. Comput. Phys. **228**, 1678 (2009).

[20] R. Saurel and R. Abgrall, A multiphase godunov method for compressible multifluid and multiphase flows, J. Comput. Phys. **150**, 425 (1999).

[21] F. Petitpas and S. Le Martelot, A discrete method to treat heat conduction in compressible two-phase flows, Comput. Therm. Sci. **6**, 251 (2014).

[22] G. Perigaud and R. Saurel, A compressible flow model with capillary effects, J. Comput. Phys. **209**, 139 (2005).

[23] D. A. Drew, Mathematical modeling of two-phase flow, Annu. Rev. Fluid Mech. **15**, 261 (1983).

[24] A. Chinnayya, E. Daniel, and R. Saurel, Modelling detonation waves in heterogeneous energetic materials, J. Comput. Phys. **196**, 490 (2004).

[25] R. Abgrall and R. Saurel, Discrete equations for physical and numerical compressible multiphase mixtures, J. Comput. Phys. **186**, 361 (2003).

[26] M. Hantke, S. Müller, and L. Grabowsky, News on baer–nunziato-type model at pressure equilibrium, Contin. Mech. Thermodyn. **33**, 767 (2021).

[27] R. Saurel and C. Pantano, Diffuse-interface capturing methods for compressible two-phase flows, Annu. Rev. Fluid Mech. **50**, 105 (2018).

[28] A. Murrone and H. Guillard, A five equation reduced model for compressible two phase flow problems, J. Comput. Phys. **202**, 664 (2005).

[29] G. Kagan and T. Xianzhu, Thermo-diffusion in inertially confined plasmas, Phys. Lett. A **378**, 1531 (2014).

[30] A. Simakov and K. Molvig, Hydrodynamic description of an unmagnetized plasma with multiple ion species. I. General formulation, Phys. Plasmas **23**, 032115 (2016).

[31] A. Cook, Enthalpy diffusion in multicomponent flows, Phys. Fluids **21**, 055109 (2009).

[32] J. D. Ramshaw and A. W. Cook, Approximate equations of state in two-temperature plasma mixtures, Phys. Plasmas **21**, 022706 (2014).

[33] C. Zhang, I. Menshov, W. Lifeng, and S. Zhijun, Diffuse interface relaxation model for two-phase compressible flows with diffusion processes, J. Comput. Phys. **466**, 111356 (2022).

[34] G. Allaire, S. Clerc, and S. Kokh, A five-equation model for the simulation of interfaces between compressible fluids, J. Comput. Phys. **181**, 577 (2002).

[35] E. Johnsen and F. Ham, Preventing numerical errors generated by interface-capturing schemes in compressible multi-material flows, J. Comput. Phys. **231**, 5705 (2012).

[36] R. J. R. Williams, Fully-conservative contact-capturing schemes for multi-material advection, J. Comput. Phys. **398**, 108809 (2019).

[37] L. Spitzer, Jr. and R. Härm, Transport phenomena in a completely ionized gas, Phys. Rev. **89**, 977 (1953).

[38] J. G. Clérouin, M. H. Cherfi, and G. Zérah, The viscosity of dense plasmas mixtures, Europhys. Lett. **42**, 37 (1998).

[39] C. Paquette, C. Pelletier, G. Fontaine, and G. Michaud, Diffusion coefficients for stellar plasmas, Astrophys. J., Suppl. Ser. **61**, 177 (1986).

[40] G. Kagan and S. Baalrud, Transport formulas for multicomponent plasmas within the effective potential theory framework, arXiv:1611.09872 (2016).

[41] V. Balashov and E. Savenkov, Classical transport equations for burning gas-metal plasmas, J. Appl. Mech. Tech. Phys. **59**, 434 (2018).

[42] K. H. Kim and C. Kim, Accurate, efficient and monotonic numerical methods for multi-dimensional compressible flows: Part ii: Multi-dimensional limiting process, J. Comput. Phys. **208**, 570 (2005).

[43] C. Zhang, H. Su, and J. Zhang, On the computation of compressible multiphase flows with heat and mass transfer in elastic pipelines, J. Comput. Phys. **490**, 112257 (2023).

[44] A. Zein, M. Hantke, and G. Warnecke, Modeling phase transition for compressible two-phase flows applied to metastable liquids, J. Comput. Phys. **229**, 2964 (2010).

[45] B. Thornber, M. Groom, and D. Youngs, A five-equation model for the simulation of miscible and viscous compressible fluids, J. Comput. Phys. **372**, 256 (2018).

[46] I. Kokkinakis, D. Drikakis, D. Youngs, and R. J. R. Williams, Two-equation and multi-fluid turbulence models for Rayleigh–Taylor mixing, Int. J. Heat Fluid Flow **56**, 233 (2015).

[47] D. Livescu, A multiphase model with internal degrees of freedom: Application to shock-bubble interaction, Phil. Trans. R. Soc. A **371**, 20120185 (2013).

[48] S. Lemartelot, R. Saurel, and B. Nkonga, Towards the direct numerical simulation of nucleate boiling flows, Int. J. Multiphase Flow **66**, 62 (2014).

[49] A. S. Richardson, *2019 NRL Plasma Formulary* (Naval Research Laboratory, Washington, DC, 2019).

[50] E. Vold, L. Yin, and B. J. Albright, Plasma transport simulations of Rayleigh–Taylor instability in near-ICF deceleration regimes, Phys. Plasmas **28**, 092709 (2021).